UNIVERSIDAD DE CONCEPCIÓN
FACULTAD DE CIENCIAS FÍSICAS Y MATEMÁTICAS
DEPARTAMENTO DE GEOFÍSICA

South American plate motion, asthenospheric flow and its implications for Andean orogeny since the late Cretaceous.

Ingo Leonardo Stotz Canales

Habilitación Profesional para optar al Título de Geofísico

Profesor Guía:
Dr. Andrés Tassara
Dr. Hans-Peter Bunge
Dr. Giampiero Iaffaldano

Comisión:
Dr. Matthew Miller, Dr. Andrés Sepulveda,

Enero de 2013

Contents

List of Figures

List of Tables

Acknowledgements

To my family for his unconditional help and support during this process: my mother Alina Canales, my father Wolfgang Stotz and my sister Gisela Stotz.

To the Universidad de Concepción for financing my studies with the scholarship "Beca Deportiva".

To the department of Geophysics of the University, the administratives and professors, for the all the valuable education given along the years. Specially to Dante Figueroa and Aldo Montecinos for the trust handed.

To the Technische Universität München and the Department of Geophysics for the scholarship given to go to Germany for a semester aboard.

To Andrés Tassara, from the Department of Geology at the Universidad de Concepción, for his support and confidence during my stay in Germany.

To Hans-Peter Bunge, chair from the Department of Geophysics at the Ludwig Maximmilians Universität, for his support this project, and all the confidence given during the process.

To Giampiero Iaffaldano, from the Department of Geophysics at the Australian National University, for all the help and support given during this process.

To the commission in charge to review this document, Matthew Miller, Andrés Sepúlveda and Andrés Tassara.

Abstract

Temporal variations of the oceanic spreading rate are an outstanding observation in the South Atlantic. The South American plate velocity record displays clear temporal velocity variations. The short duration of the South American plate velocity changes makes it difficult to attribute them to variations of the large-scale mantle buoyancy distribution, which evolves on longer time scales on the order of 50 to 100 Ma. However, geologic processes such as the creation of high elevated topography (orogeny) vary in a short time scale, on the order of 20 Ma. By a simple force balance analysis between the boundary forces (e.g ridge push, friction and Andean forcing) and the basal shear forces (e.g., pressure driven (Poiseuille) asthenosphere flow), the hypothesis to test is that the Andean orogenic evolution can explains the velocity variations and that the South American plate motions are driven by basal shear forces related to pressure driven (Poiseuille) low viscosity asthenosphere flow beneath the lithosphere, with an estimated flow velocity on the order of 10 cm/yr at present day to balance with the other forces, considering a channel thickness of 250 km and a viscosity of 1×10^{19} Pa s. Our results show that in order for the evolution of the elevation on the Andean topography to explain the velocity variations observed, the Andes should have for the past an high elevated topography. The geological record of the Andes, disagrees with our results. Because geological information shows that the Andes did have a low topographic elevation for past times, and that higher elevations were reached in a later stage. We tested our consdirations on the thickness and viscosity of the asthenospheric channel by comparing them with independent information sources (e.g., seismic tomography and the geoid), finding consistency. Pressure gradients affects asthenospheric flow velocities, due to lateral topographic variations (e.g Dynamic topography). The pronounced dynamic topography gradient across the South Atlantic region (e.g., African superswell), implies significant westward flow in the asthenosphere. This new hypothesis is tested using a Poiseuille flux in the asthenosphere, resulting in a flow velocity variation on the order of 10 cm/yr, this value is comparable to asthenosphere flow velocities estimated to balance present day Andean topography. Results shows that vertical plateau motions, have important implications on plate motions. Thus, our novel approach contributes to a more integral understanding of plate motion, not only due to boundary forces, but also by basal shear forces and the influence of far field effects, such as dynamic topography in the adjacent plates.

Chapter 1

Introduction

The South Atlantic holds a prominent place in the history of plate tectonics from the time when Bullard *et al.* (1965) proposed a fit of South America and Africa which convincingly showed how both continents were once joined. Owing to its passive margin environment the South Atlantic preserves an exceptional archive of past plate motion (see Fig. 1.1 for an age model from Müller *et al.* (2008b), and the spreading history of the basin is known in considerable detail (Cande *et al.* 1988 and Nurnberg & Müller 1991).

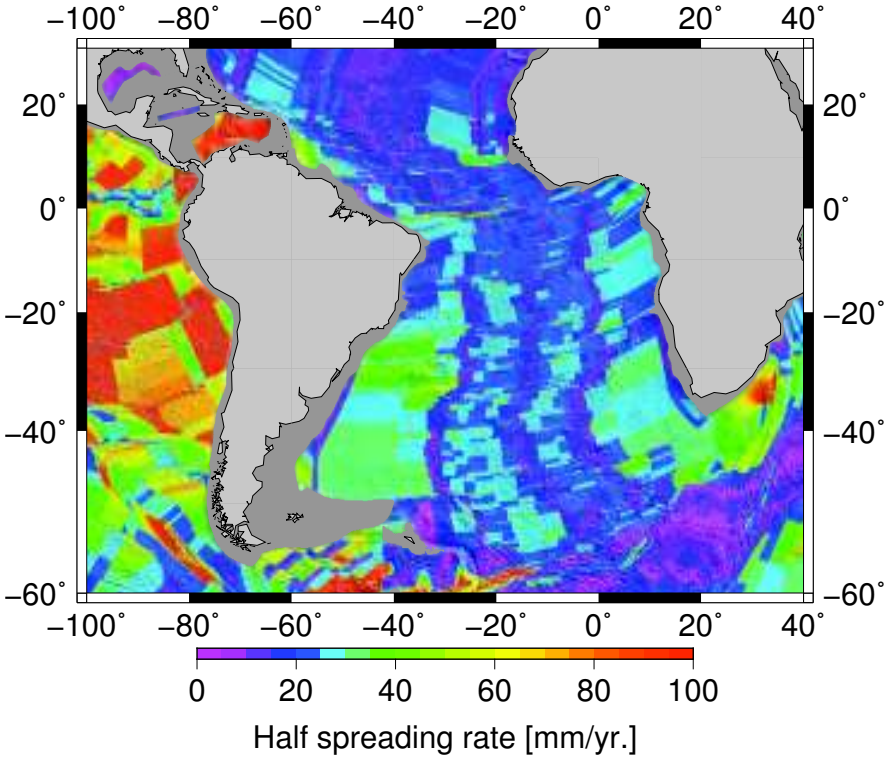

Figure 1.1: *Half-spreading rates of conjugate plates from* Müller et al. *(2008a).*

Temporal variations of the oceanic spreading rate are an outstanding observation in the South Atlantic. Figure 1.1 shows ocean floor spreading half-rates of the South Atlantic taken from the recent global compilation of Müller *et al.* (2008b) on the basis of marine magnetic anomaly identifications and following the techniques outlined by Müller *et al.* (1997). The compilation reveals abrupt velocity changes over time-periods of a few Ma. The velocity changes shown in Fig. 1.2 are two velocity slowdown and velocity increase. The first velocity down, at 80 Ma, is of 3 cm/yr on a time interval of 20 Ma, while the second is a gradual velocity slowdown during the last 40 Ma. Although it is accepted that buoyancy forces associated with subduction of cold, dense lithosphere provide significant driving forces for plate motion, the short duration of the South Atlantic spreading rate changes makes it difficult to attribute them to variations of the large-scale mantle buoyancy distribution, which evolves on longer time scales on the order of 50 to 100 Ma for a velocity change of $\Delta v = 1$ cm/yr, as suggested by mantle circulation modelling (Bunge *et al.*, 1998), for further reading refer to appendix B.

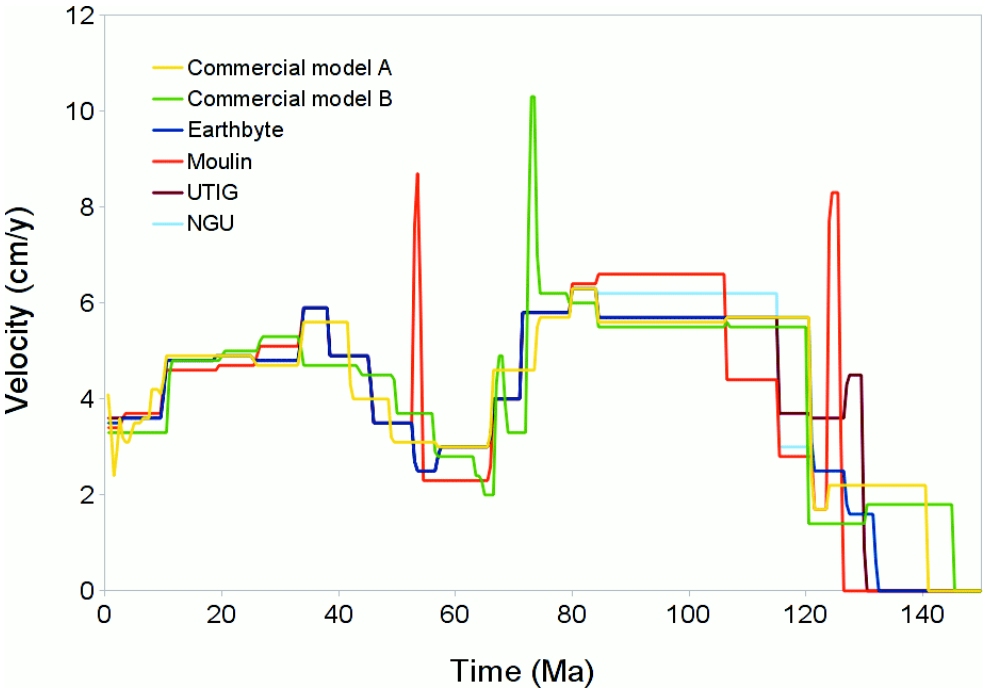

Figure 1.2: *Spreading velocity record for South America with respect to Africa (Africa fix). The velocity record reveals short time velocity variations that can not be attributed to large-scale mantle buoyancy forces. The x-axis shows the time scale since Cretaceous (140 ma) to the present (right to left, respectively) and the magnitude of the velocity in the y-axis. The color lines represents the different model used to constrain the data (Bianchi* et al., *2011)*

The South Atlantic is also an area of anomalous topography with a pronounced bathymetric asymmetry (Fig. 1.3), and buoyant flow rising from the deep mantle might be a significant factor shaping the regional tectonic evolution. It is well known that the mantle beneath Africa has long been shielded from subduction by the former supercontinent Pangea (Anderson, 1982). The sub-African mantle, moreover, harbours one of the world's major low-seismic velocity bodies (e.g., Simmons & Grand 2002, Tkalcic & Romanowicz

2002, Simmons *et al.* 2007 and Nyblade & Robinson 1994). Much of the seismic wave-speed reduction in this anomalous mantle body is probably due to highly elevated temperature (Schuberth *et al.*, 2009). Thermal upwellings are thus entirely expected to play a prominent role in the South Atlantic, consistent with observations of numerous plume related volcanic centres (see Fig. 1.4), elevated heat flow in the mobile belts of southern Africa, and inferences that Africa experienced greater uplift than other continents in the Tertiary (e.g., Burke & Gunnell 2008).

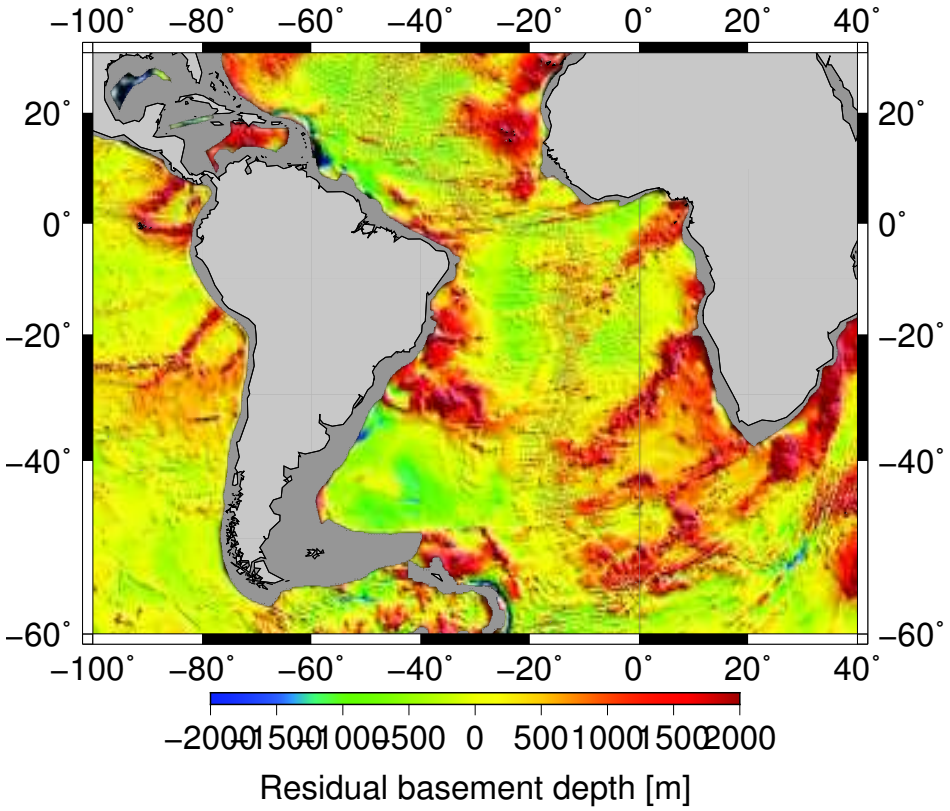

Figure 1.3: *Residual basement depth grid computed by calculating the difference between the predicted basement depth and the sediment unloaded basement depth. Predicted basement depth is obtained by applying Crosby et al.'s (2006) North Pacific thermal boundary layer model to the age-area distribution from Müller* et al. *(2008a).*

Strongly plume-driven tectonic activity in the South Atlantic region agrees well with recent geodynamic considerations on the mantle energy budget. Several modelling studies (e.g., Bunge *et al.* 2001, Zhong & Leng 2006) now advocate a prominent role of active thermal upwellings in the mantle general circulation, accounting for as much as 30 percent ($10TW$) of the total mantle heat loss. This value is considerably larger than what was inferred earlier from arguments based on the dynamic topography over hot spots (Davies, 1988).

Some South Atlantic spreading rate changes undoubtedly reflect temporal variations in plate boundary forcing, in particular along the active western margin of South America. The most significant tectonic

change in the region over the past 25 Ma is the growth of the high Andes, especially the rise of the Altiplano and Puna plateau some 10 Ma ago (e.g., Garzione *et al.*, 2006, Gregory-Wodzicki 2000, Charrier *et al.* 2007). Estimates for the tectonic forces associated with the current Andean topography amount to $\sim 8\times10^{12}$ N/m on average, comparable to the driving forces in plate tectonics (Husson & Ricard 2004 and Iaffaldano *et al.* 2006). The temporal correlations between Andean uplift and plate kinematic changes around South America support the notion that the load of this newly elevated topography affected plate motions in the South Atlantic region. For instance, the 30 percent convergence velocity reduction across the Nazca/South America margin in the late Miocene, commonly attributed to growth of the high Andes (e.g., Norabuena *et al.* 1999), has been linked explicitly to a corresponding reduction of South Atlantic spreading rates in a global coupled model of the mantle/lithosphere system (Iaffaldano *et al.*, 2006). Far field effects are thus an important factor influencing the South Atlantic spreading record. Husson *et al.* (2012), moreover, attributed the most recent South Atlantic spreading rate reduction to the formation of an optimal aspect ratio in a deep mantle circulation cell beneath the South Atlantic.

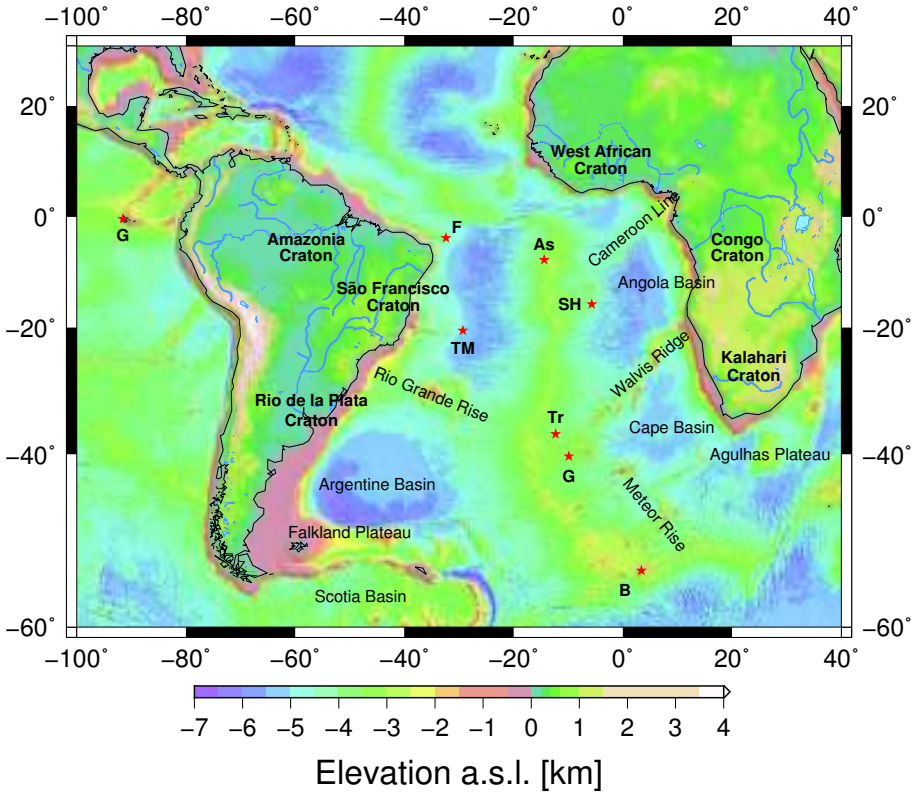

Figure 1.4: *Topographic map of the South Atlantic and adjacent continents from ETOPO1 (Amante & Eakins, 2009), annotated with major structural elements cited in the text. Craton names are boldface, while stars denote prominent hotspots (F: Fernando de Noronha; As: Ascension; Af: Afar; SH: Saint Helena; TM: Trinidade and Martim Vaz; Tr: Tristan da Cunha; G: Gough Island; B: Bouvet Island; M: Marion; C: Crozet Islands)*

Rapid spreading rate changes, observed in Fig. 1.2, suggest a significant decoupling of plate motion from the large scale mantle buoyancy distribution, as noted before, presumably through a mechanically weak layer known as asthenosphere. An asthenosphere was advocated early on in the history of plate tectonics to lubricate plate motion. Abundant evidence for the asthenosphere comes from a variety of observations, including the Geoid (e.g., Hager & Richards 1989), glacial rebound (e.g., Mitrovica & Forte 2004), oceanic intraplate seismicity (e.g., Wiens & Stein 1985), ocean ridge bathymetry (e.g., Buck *et al.* 2009), seismic anisotropy (e.g., Debayle *et al.* 2005). While the cause for low mechanical strength of the asthenosphere is probably due to weakening effects associated with partial melt and/or water (e.g.,Karato & Jung 1998), consequences include a concentration of upper mantle flow into a narrow channel of greatly enhanced material mobility. Fluid dynamic considerations based on numerical and analytic models (e.g., Bunge *et al.* 1996) confirm that high material mobility in the asthenosphere is essential to promote the unique long wavelength pattern of mantle flow observed on Earth.

Morgan *et al.* (1995) argued for asthenosphere flow with a pressure driven component due to plumes, which would explain a variety of observations related to mantle geochemistry, heat flow and ocean bathymetry. In a series of remarkable papers, Hoeink and Lenardic (2008, 2010, 2011) substantiated this idea. They predicted that plate motion in the South Atlantic region arises predominantly from basal shear forces related to pressure driven (Poiseuille) asthenosphere flow (Hoeink *et al.*, 2011). The concept of asthenospheric flow driven by high and low pressure regions is productive. It relates spreading rate changes driven by evolving basal shear forces explicitly to non-isostatic vertical motion known as dynamic topography, which one can test with independent data. In fact, Japsen *et al.* (2012) (and references therein) has drawn attention recently to episodic burial and exhumation of passive continental margins. Such events are documented along the Brazilian coast and are difficult to understand in terms of a simple lithosphere cooling process, presumably reflecting temporal changes in dynamic topography, which refers to topography generated by the motion of zones of differing degrees of buoyancy (convection) in the Earth's mantle.

Consequently, the hypothesis to test is that the South American plate motions are driven by basal shear forces related to pressure driven (Poiseuille) low viscosity asthenosphere flow beneath the lithosphere. And the plate velocity variations are related to the Andean orogenic evolution (e.g paleoelevation) along the west boundary of the South American plate. Thus, the objectives are,

- Understand and quantify the forces acting on the South American plate.
- Using a force balance estimate the paleo elevation of the Andes.
- Reconstitute the geologic evolution of the Andes base on the available literature, to have a geologic paleo elevation of the Andes.
- Compare both results to test the hypothesis.

However, far field effect (e.g., African plateau evolution (Janssen *et al.*, 1995)) may play also a prominent role into the South American plate motions.

To test the hypothesis and achieve the objectives the document will be divided into 5 more chapters. Chapter 2, the methodology, will explain how to confront the problematic. Chapter 3, geology of the Andes, will be described the orogenic evolution of the Andean Cordillera. In chapter 4, the force balance, will be estimated the paleo elevation of the Andes. In chapter 5, discussion, results are going to be compared and discussed. Chapter 6 is the conclusion.

Chapter 2

Methodology

1 The South American plate motions are controlled by driving and resisting forces. The latter are the Andean forcing, due to his topographic elevation, and the frictional forces along the convergent margin. While the driving forces are the Ridge push, a gravitational force, and the basal shear forces related to the asthenospheric flow. Quantification of this forces will allow us to describe South American plate motions.

2 Our model calculations will be as simple as a force balance, in which for each time interval the sum of all forces equals zero, because acceleration in the solid Earth are negligible. To solve it a Maltab based code will be use. The plate will be treated as a particle to which forces are applied. Each force will be applied either to the whole plate or to its borders, therefore summing all contribution will be made to get one value for each force. The frictional and ridge push forces are know from the literature (e.g., Fowler 2009). The Andean forcing was already estimated by Iaffaldano *et al.* (2006). But the basal shear force related to the asthenospheric flow depends on parameters that can not be measured in situ. For present day conditions the ridge push, frictional and Andean forcing forces are know. With this, we can estimate the parameters needed characterize the basal shear forces in order to be in balance with all the other forces, however, they are not unique. Detail of all the calculations and assumption are described in the chapter 4.

3 Knowing all the parameters to quantify the forces acting on the South American plate we can estimate the Andean topographic elevation for the past in order to describe the velocity record observed (see Fig. 1.2). The low velocities observed are related to high elevation in the Andean topography, while the fast velocities are related to low elevation in the Andean topography. Due to the fact the parameters for the basal shear forces related to the asthenosphere flow are not unique, we will obtain a variety of solutions. Independent information sources (e.g., Seismic data) are going to be use to restrict the parameters and find the most reasonable solution.

4 From an extensive literature review, the Andean paleo elevation history for the last 100 Ma will be made, based on the geological records. All the geological information is sorted in the table C.1 to facilitate its comprehension. The contents of the table are the name of the author (reference), the type of

information, location, time periods and the main features discussed in the article. With all this is easier to recall the important information of each article. And in chapter 3.

5 Both results are going to be compared to validate our estimation of the Andean paleo elevation. If the orogenic history of the Andes since 100 Ma does explain the velocity variations observed in the velocity record, then our estimation of the paleo elevation of the Andean topography should coincide with elevation of the Andes based on the geological records. In case both results qualitatively coincide, then the hypothesis will be accepted. In contrary case, then the hypothesis will be rejected and an other process will be discussed to explain the South American velocity variations.

Chapter 3

Geology of the Andes

3.1 Anatomy of the Andes

The Andes is one of the major Cordillera in the world, it extends from far north ($\sim 7^oN$) to the end of the Continent far south in the Tierra del Fuego (ca 55^oS). The average topographic elevation in the Central Andes is on the order of 4 km and its mayor mountain is the Aconcagua, at $\sim 30^oS$, reaching an elevation of ~ 7 km.

The Andes display considerable latitudinal variation and are therefore divided in three zones (Gansser 1973, Tassara & Yanez 2003 and Sempere *et al.* 2008), as can be see in Fig. 3.1. The Northern Andean goes from $\sim 12^oN$ to $\sim 5^oS$. The Central Andean, the largest and most voluminous segment t present day, goes from $\sim 5^oS$ to $\sim 37^oS$ and is also subdivided into three regions, the North Central Andes, Central Orocline and South Central Andes. The Central Andes are characterized by the dominance of protracted magmatic activity in the west (widely distributed around the Western Cordillera, i.e. the arc) and by tectonic shortening in the east (in the Eastern Cordillera and adjacent areas). As a whole, the Central Andes form a major segment of continental arc and display extraordinary characteristics and noteworthy internal longitudinal gradients (Sempere *et al.*, 2008). The Southern Andean goes from $\sim 37^oS$ to the end of the continent at $\sim 55^oS$ and are characterized by a 2000 km long belt of granitoids hosted along their axial part, named as the Patagonian batholith (Folguera *et al.*, 2011). Given that the aim of this study is to describe the geological evolution of the Andean topographic elevation, the main focus of our work lays on the Central Andes, where the main geological processes related to topographic construction have occurred in the last 100 Ma, since late Cretaceous (Geological time scale is available in appendix A).

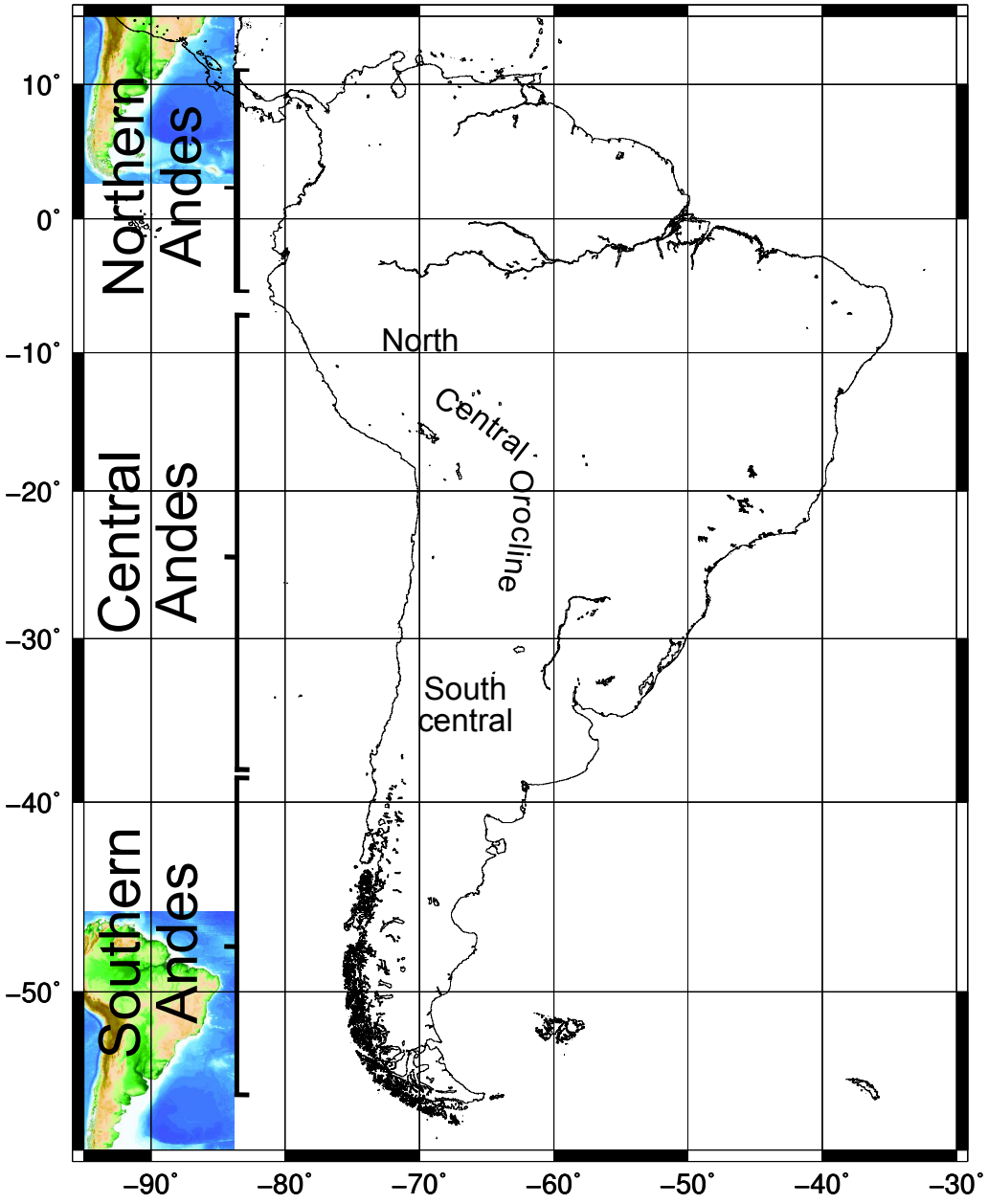

Figure 3.1: *Topographic map of the South American continent and its most prominent geological feature, the Andes. The Andean Cordillera extends along the whole continent from north to south. The Andes is also segmented in three main zones the Central, South and North. Further the Central Andean Zone, is separated also in three regions the North, Central Orocline and South-central. (Gansser, 1973)*

Each region of the Central Andes contains important geological features and structures. The Northern Central Andes describes several important geological structures, such as the Coastal Cordillera, the Coastal and Western Through, the Axial swell and the Eastern basins (Jaillard, 1994), see Fig. 3.2. The Central Orocline has many important geological structures. From west to east, the central depression is

between the Coastal and Pre Cordilleras, east from this latter is the Salar de Atacama surrounded from the west by the Western Cordillera (Mpodozis *et al.*, 2005). East from latter, lays the Altiplano and Puna plateau, a $\sim$4 km high structure. This two structures are easterly closed by the Eastern Cordillera. The eastern most structure is the Subandean region (Gregory-Wodzicki, 2000). The Southern part of the Central Andes is characterize by the Frontal Cordillera that goes from $\sim 26^oS$ to far south, which contain the Aconcagua mountain, the highest one along the Andes, up to $\sim$7 km high (Sempere *et al.*, 1994).

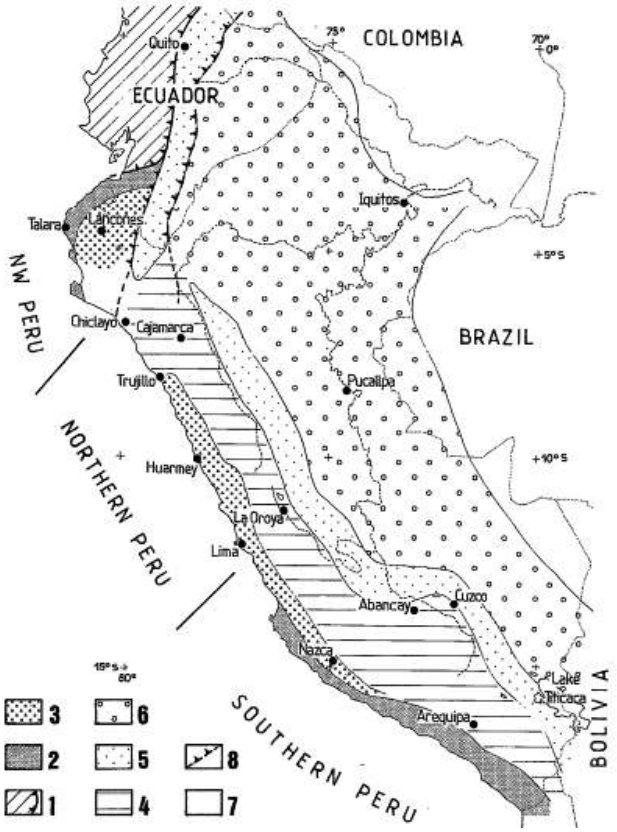

Figure 3.2: *Paleogeographic sketch of the Peruvian margin, and location of main areas cited. 1: Cretaceous allochthonous terranes, and suture. 2: Coastal Cordillera. 3: Coastal Troughs. 4: Western Trough. 5: Axial Swell. 6: Eastern Basin. 7: Brazilianand Guianese (Colombian) Precambrianshields. 8: Jurassic suture (Jaillard, 1994).*

3.2 The Andean evolution

The pre-Andean cycle started in late Pre-Cambrian until early Jurassic (200 Ma), were the Andean tectonic cycle started. During the pre-Andean cycle subduction was not active, however terrains were accreted to the pre-Andean margin, such as Pampean terrane, Precordillera terrane and the Patagonia terrane (Rapela *et al.*, 1998). The Andean cycle started by early Jurassic, which we are interested, and can be divided into two periods, an early and late period (Charrier *et al.*, 2007).

ANDEAN TECTONIC CYCLE

PERIODS*	STAGES**	SUBSTAGES**	AGE
Late Period	Third Stage		Late Paleogene to Present
	Second Stage	Second Substage	Early Paleogene (Paleocene-Early Eocene)
		First Substage	late Early Cretaceous to Late Cretaceous
Early Period	First Stage	Second Substage	Kimmeridgian-Tithonian to Albian
		First Substage	late Early Jurassic to Kimmeridgian

* Subdivision according to Coira et al. (1982)
** Subdivision according to this work

Figure 3.3: *Andean tectonic cycle, since early Jurassic (Charrier* et al.*, 2007)*

For what concerns to our study, we are interested into the late period of the Andean tectonic cycle, since late Cretaceous, where the main tectonic processes related to the orogeny of the Andes occurred. However, it is important to know taht during the early period of the Andean cycle, it was dominated by extensional setting along the Andean margin (Charrier *et al.*, 2007).

The orogenic evolution of the late period of the Andean evolution has been long studied, however it is still under debate, due to its complexity. Traditionally, three main phases of Andean orogeny are accepted (Steinmann *et al.*, 1929). These phases are the Peruvian during late Cretaceous, Incaic or Inca in middle Eocene and Quechua since late Miocene. The Peruvian phase has also been described by Jaillard & Soler (1996) and Charrier *et al.* (2007) among others, beeing in temporal and spatial agreement with Steinmann *et al.* (1929). For the Inca phase the story is a bit different, because Sempere *et al.* (1990) argued that this phase occurred actually in late Oligocene instead of middle Eocene. However, lately consensus was reached in that tectonic activity started slowly in middle Eocene reaching its maximum during late Oligocene (Sempere *et al.*, 2008). The Quechua phase, since late Miocene to present, concentrates principally in the Central Orocline (e.g Altiplano and Puna) (e.g., Garzione *et al.* 2006, Ghosh *et al.* 2006 and Gregory-Wodzicki 2000), where the Andes reached its actual development. In latest late Cretaceous to early Paleocene a main short-lived tectonic event took place, in the Central Orocline and Southern Central Andes, named the K-T event (Cornejo *et al.* 2003 and Charrier *et al.* 2007).

During late Cretaceous the geological record in North Central Andes documents tectonic processes along the margin related to the first Andean orogenic phase, the Peruvian, named after the Peru region between 5^oS and 17^oS (e.g., Steinmann *et al.* 1929, Jaillard 1994 and Charrier *et al.* 2007 among others). The Peruvian phase, described by Jaillard (1994), is composed by three stages, the first in the Turonian to Coniacian boundary (89 - 88 Ma), the second in late Coniacian to earliest Santonian (87 - 86 Ma) and a third one in late Campanian (76 - 73 Ma).

The first stage was related to an incipient coastal uplift and inversion of the previous subsidence of the Coastal area. Directly after it, the second stage was related to tectonic activity with compressional strain in the directions NE-SW. More generally an increase in the compression in the Coastal area, associated with lateral movements, that ended uplifting the margin. This uplift provoked a retreat of the sea during late Santonian. Later, the third stage was related with thrusting and fore land sedimentary deposits. Accordingly, in north-western Peru, the deposition of sediments indicates a marked paleogeographic change, characterized by the uplift and erosion of the Coastal Cordillera and the sinking of the coastal area, thus expressing the creation of the first late Cretaceous forearc basin in the coastal zone of northern Peru. Therefore, with this evidence it could be inferred that an orogenic process highly related to mountain uplift occured (Jaillard, 1994). Additionally Jaillard & Soler (1996) and references therein described a major contractional event in the south-western Peru during late Campanian.

These tectonic processes in the Northern Central Andes identified as a regional event also correlates with similar processes along the whole Central Andean margin. In the Central Orocline, specifically in Bolivia and north-western Argentina, three stages of tectonic activity (Sempere *et al.*, 1997). The first of stages (89 Ma) correlates with the Peruvian phase. Thus, from stratigraphy data it can be inferred that in late Turonian to Campanian (89 to 73 Ma) a tectonic event marked the turning point in Andean evolution in the Northern Central Andes and foreland conditions east of the Andes domain prevailed. Furthermore, in the Salar de Atacama, $\sim 23^o$ S in the Atacama region in Chile, during late Cretaceous (70 Ma) an uplift in the Cordillera Domeyko, west to the Salar de Atacama basin, was found, based on the high sedimentation rates on the Salar basin (Mpodozis *et al.*, 2005).

In the Southern Central Andean correlation with the Peruvian tectonic phase was also found. In the Neuquen basin, at $\sim 38^o$ S on the eastern foreland domain of the Andes, evidences of tectonic events in late Cretaceous (Tunik *et al.*, 2010), which argue based on fission track data, detrical zircons and biostratigraphic evidence that the beginning of Andean uplift for this area can be bracketed between Cenomanian and Coniacian. Additionally, in the same area stratigraphical and structural evidence suggest a compressional deformation setting from Aptian to Campanian (Tunik *et al.*, 2010).

Tectonic activity during late Cretaceous along the Central Andean margin, was followed since late Campanian by a tectonic quiescence, probably by extensional settings. Also during Maastrichtian marines transgressions were found in the Central Orocline. In latest late Cretaceous and early Paleocene (65 Ma) this tectonic quiescence was interrupted by a major short lived tectonic event, the K-T event, in the Central Orocline (Cornejo *et al.*, 2003).

This K-T event, was first documented by Cornejo *et al.* (2003) in the Central Orocline, were she did find a series of unconformities, between late Cretaceous and the overlying Paleocene strata, in a wide region from 20^oS to 26^oS. Later Charrier *et al.* (2007) described also this short lived tectonic event and found correlation with deformation processes up to the region of Concepcion at $\sim 36^oS$.

More evidence supporting this event, is observed in the North Central Andes, north from the Altiplano near the Titicaca lake in the Vilquenchico area $\sim 15^oS$, where Jaillard *et al.* (1993) described an angular

unconformity dated late Maastrichtian. Further, in the Cajamarca and southern-east Ecuador regional compression processes were recorded in the stratigraphic data (Jaillard & Soler, 1996).

In the Southern Central Andes, in the Neuquen basin correlations to tectonic events are closely related to the Peruvian phase in late Cretaceous, although by a narrow age margin this events can be also related to the K-T event (Cobbold & Rossello, 2003). In the Southern Andes, Aragon *et al.* (2011) described the development of a proto Andean range in the Patagonian area indicating correlation with the Peruvian phase.

After the K-T event that ended in early Paleocene, extensional settings resumed in the Central Andes, but with less intensity compared to early Cretaceous (Charrier *et al.* 2007 and Jaillard & Soler 1996).

The second phase of Andean evolution is the Inca. This orogenic phase developed, presumably, first by a slow start in the middle Eocene, followed by a peak in tectonic activity by late Oligocene (Sempere *et al.*, 2008). During middle Eocene in the Central Andean Plateau (e.g Altiplano and Puna), Gillis *et al.* (2006) base on fission tracks dated the time periods of rapid cooling (e.g exhumation), which are related to uplift processes. He found and described two periods of rapid cooling, the first fast cooling period started in middle Eocene (45 Ma to 40 Ma) and continued throughout late Eocene and Oligocene and ended by $\sim$ 26 Ma. The second period of fast cooling started in late Miocene ($\sim$ 11 Ma). Barnes *et al.* (2006) found similar results for the same area.

In late Oligocene, Sempere *et al.* (1990) described a major tectonic crisis in the Central Orocline that resulted in the development of the Subandean external foreland basins and the intermontane basins in the Altiplano, which where separated by the thrusting and uplift of the Eastern Cordillera. Horton (2005) emphasised that in late Oligocene the development of the intermontane basin fill started in the Altiplano region, bounded by the Eastern Cordillera to the east, and were deposited forming an angular unconformity. Furthermore, McQuarrie *et al.* (2008) based on apatite fission track described the amounts and time of deformation and crustal shortening in the Central Orocline, dating from late Eocene to Oligocene a fast exhumation period in the Eastern Cordillera, presumably related to uplift. Arriagada *et al.* (2008) reached similar results, reporting that the Central Orocline was formed between late Eocene and Oligocene based on apatite fision tracks.

In the Northern Central Andes during late Eocene and Oligocene Jaillard & Soler (1996) described folding and inverse faulting in the Western Through, that runs near the coastal area along the entire Peruvian region, that ended forming a fold and thrust belt. Further, in the North Central Andes Picard *et al.* (2008) dated the Andean elevation using phylogenetics of highland biotaxa. Results show that by early Miocene (23 to 19 Ma) the Southern most part of the Northern Central Andes reached 2 to 2.5 km and that the uplift propagated northward, reaching the same elevation in the central part of the Northern Central Andes by middle Miocene. Later in the late Miocene these elevations were also reached in the northern most part of the North Central Andes. Thus, these results showed that uplift in the Central Andes, presumably started in the Central Orocline by late Oligocene and then propagated north and south from it, as can be see in Fig 3.4.

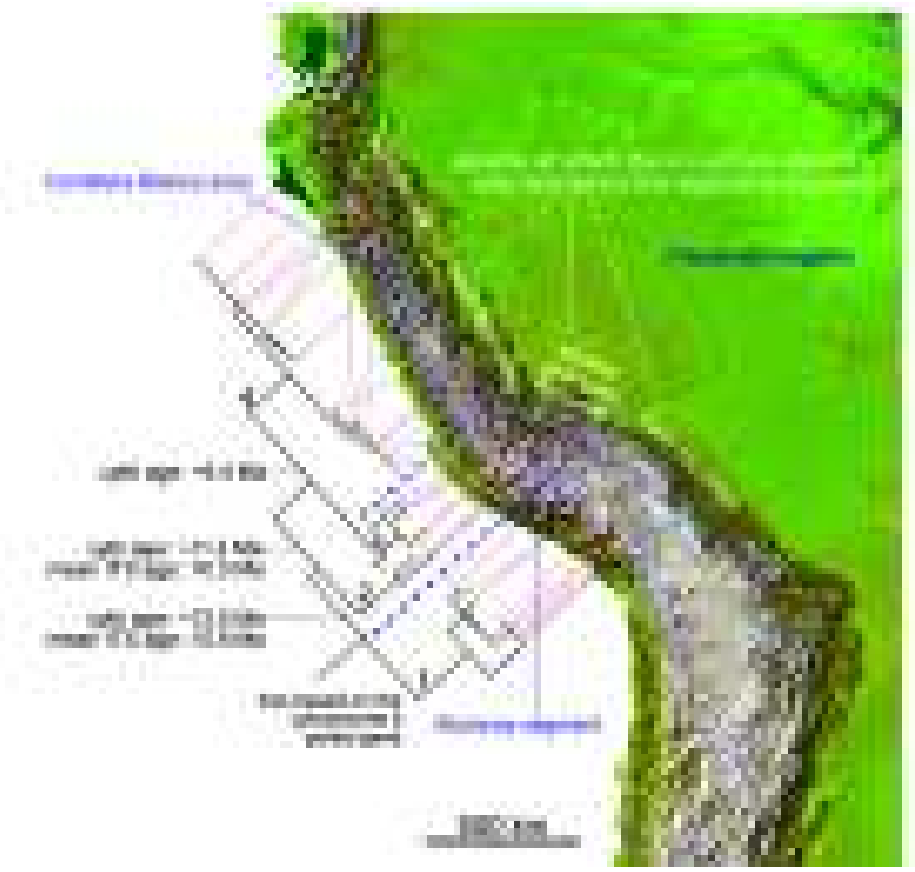

Figure 3.4: *Timing and propagation of Andean uplift from southern to northern, in the Northern Central Andes (Picard* et al.*, 2008).*

In the Central Orocline Gregory-Wodzicki (2000), based on paleobotanical, fission track and geomorphological data, dated the initiation of uplift in the Western Cordillera by early Miocene, where it may have reached half of its present elevation. Additionally, the Altiplano should have reached a third of its present elevation by the same time, and half of it by 10 Ma. For the Eastern Cordillera she found that it had reached half of its actual elevation by 10 Ma (Gregory-Wodzicki, 2000).

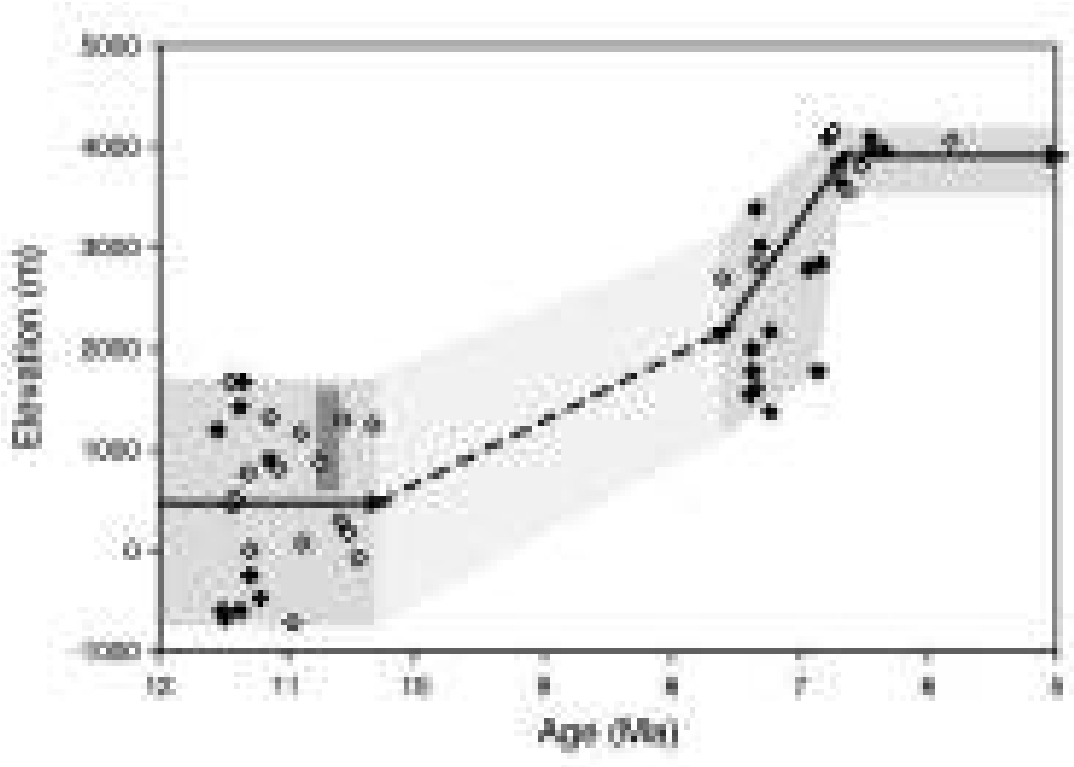

Figure 3.5: *Compilation of paleoelevation estimates from oxygen isotopes in carbonates (medium gray) and paleoleaf physiognomy (dark gray bar). Open diamonds are estimates from paleosol carbonates, and closed diamonds are palustrine carbonates. Paleoelevation estimates from both fossil leaves and carbonates prior to* $\sim$ 10.3 *Ma overlap in range and indicate that no more than half of the modern elevation was achieved. Paleoelevation constraints are lacking between 10.3 Ma and* 7.6 *Ma (light gray), during the time period of widespread lacustrine deposition within our section. Based on O isotopes, uplift of* $\sim$ 2.5 *to* $\sim$ 3.5 *km occurred between* $\sim$ 10.3 *and* 6.8 ± 0.4 *Ma isotopes, followed by similar to modern elevations in the Altiplano (Garzione* et al.*, 2006).*

Most authors argue that the Andes hab its mayor development during the last 10 Ma, in the Quechua phase (Steinmann *et al.*, 1929). These assumptions are based on paleosol carbonates (Ghosh *et al.* 2006 Garzione *et al.* 2006) and fission tracks (Gillis *et al.* 2006 and Barke & Lamb 2006). Rapid cooling commenced at $\sim$ 11 Ma in the Andean Orocline (Gillis *et al.*, 2006). In the Eastern Cordillera is estimated that uplift processes started between $\sim$ 12 to $\sim$ 9 Ma (Barke & Lamb, 2006). Garzione *et al.* (2006) estimated the approximated elevation in the Central Orocline, specifically in the Altiplano region, using oxygen isotopes in carbonates, paleosol and palustrine carbonates and paleoleaf physiognomy. Her results show that by $\sim$10 Ma the elevation was less than half when compared to present day, as shown in Fig. 3.5. However, these results were argued by Hartley *et al.* (2007) due to the high uncertainty of the methods used and by the other stratigraphic evidences that points that the Andes development started earlier than late Miocene (Sempere *et al.*, 2006).

Thus, as reviewed above, there is a strong body of information supporting the development of the Andes in 3 stages. A first periods in late Cretaceous to early Paleocene, where tectonic activity commenced in the Northern Central Andes by late Cretaceous and propagated south to the Central Orocline, place where a major tectonic event closed this first stage by early Paleocene. However, elevation of the Andes by this time in these regions was presumable low, in an opposite scenario more prominent geological features related to uplift processes should be expected. Later, in middle Eocene the second stage of Andean orogeny started slowly to develop in the Central Andes, until it reached its maximum during late Oligocene even early Miocene. And the later orogenic stage started in late Miocene to present and appears to be more vigorous.

Chapter 4

Force balance for South America

The South American plate is moving westward since the split of the Gondwana continent ∼140 Ma ago. The forces acting on the plate are the friction along the convergent margin, the Andean forcing, the ridge push and the basal shear tractions. The first two forces resist the movement of the South American plate to the west, while the last two drive the plate westward. All the forces are illustrated in the Fig. 4.1.

The force balance equation will consider the four forces mentioned above and since the Earth is round we will use the torque instead of the force, $\vec{M} = R \times \vec{F}$, where R is the radius of the Earth. Thus,

$$\vec{M}_{fr} + \vec{M}_{mb} + \vec{M}_{rp} + \vec{M}_{bd} = 0 \tag{4.1}$$

Where $\vec{M}_{fr}$ states for frictional torque at the convergent boundary of the plate, $\vec{M}_{mb}$ is the Andean forcing torque, $\vec{M}_{rp}$ is the ridge push and $\vec{M}_{bd}$ is the basal shear torque related to the asthenospheric flow.

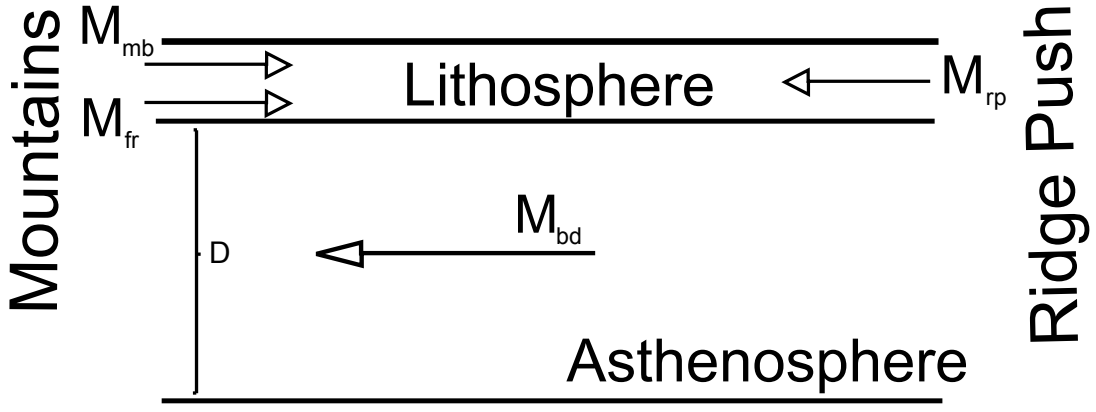

Figure 4.1: *A sketch of the South Atlantic region, displaying the driving (arrow pointing to the left) and resisting (arrow pointing to the right) forces. The forces are the ridge push $\vec{M}_{rp}$, basal shear traction $\vec{M}_{bd}$, friction force $\vec{M}_{fr}$, Andean forcing $\vec{M}_{mb}$.*

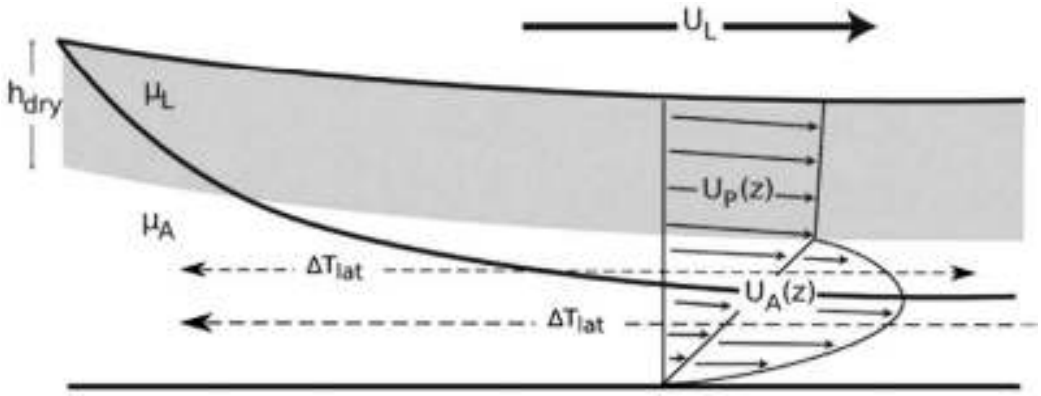

Figure 4.2: *Sketch of the pressure driven (Poiseuille) flow in the asthenosphere (Hoeink* et al.*, 2011).*

4.1 Forces that drive plate motions

The driving forces are the forces that promote plate movements. This two are the basal shear tractions and the ridge push. The first one is a force that is caused by the shear traction done below the lithosphere due to a high velocity flow (faster than the plate velocity) in a low viscosity asthenospheric channel (Hoeink *et al.*, 2012). The second is the force at the mid-ocean ridge on the edge of the plate, due to the pushing by the upwelling mantle material and the tendency of newly formed plate to slide down the sides of the ridge (Fowler, 2009). Our calculation will be done under the assumption of the existence of a thin low viscosity asthenospheric channel beneath the lithosphere (Hoeink & Lenardic, 2008), see Fig. 4.2.

The basal shear traction strongly depends on the characteristics of the asthenospheric flow, viscosity and the thickness of the channel. The shear stress τ is define as a force per unit of area, which equals the viscosity μ times the deformation ε over a time interval. This, at the same time, is equivalent to a velocity change over distance $\frac{\Delta v}{\Delta x}$. Since, the shear stress is a force per unit of area, we can integrate over the area to obtain the force, as can be seen below,

$$\begin{aligned} \tau &= \mu \frac{\Delta v}{\Delta x} \\ \vec{F}_{bd} &= \int \tau dA = \int \mu \frac{\Delta v}{\Delta x} dA \\ \Delta v &= \vec{R} \times \Delta \vec{w} \end{aligned}$$

Where $\Delta x = D$ is the depth to the maximum velocity, see Fig. 4.2, of the asthenospheric flow and $\vec{w}$ is the euler vector of the velocity. Now to obtain the Torque, force to unit length, we just need to make the cross product of this force with respect to the centre of the Earth $\vec{R}$, which leads to,

$$\begin{aligned} \vec{M}_{bd} &= \int \vec{R} \times \frac{\mu}{D} \left(\Delta \vec{w} \times \vec{R} \right) dA \\ \Delta \vec{w} &= w_{ast} - w_{plate} \end{aligned}$$

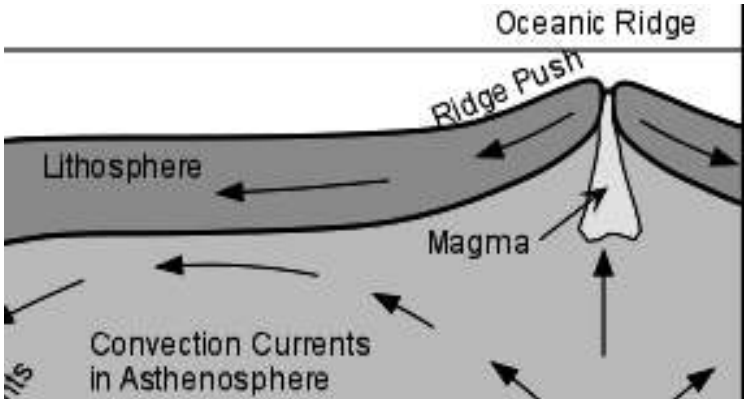

Figure 4.3: *Sketch of the ridge push force.*

$\vec{R}_b$ and $\vec{R}_d$ are defined as the distance from the centre of the Earth to the base of the lithosphere and to the surface of the lithosphere, respectively. With a lithospheric thickness depending on the age of the oceanic plate, which varies between 30 km to 100 km, approximately.

$$\vec{M}_{bd} = \int \vec{R}_d \times \frac{\mu}{D}\left((w_{ast} \times \vec{R}_b) - (w_{plate} \times \vec{R}_d)\right) dA \qquad Nm \tag{4.2}$$

The equation 4.2 represents the shear traction done by the asthenospheric flow at the base of the lithosphere, this traction drives the plate into the same direction of the flow in the asthenosphere. Where w_{plate} is the observed plate velocity and w_{ast} is the flow velocity in the asthenosphere and A is the size of the plate, which is know from present and past times.

As an example, Hoeink and Lenardic (2008,2010) showed successfully that the basal shear tractions done by the asthenosphere can drive plate motions using values of thickness and viscosity on the order of 100 km and 10^{19} Pa s, respectively.

The ridge push is the force at the mid-ocean ridge on the edge of the plate, due to the pushing by the upwelling mantle material and the tendency of newly formed plate to slide down to the sides of the ridge (Fowler, 2009), see Fig. 4.3.

$$\vec{F}_{rp} = ge(\rho_m - \rho_w)(\frac{L}{3} - \frac{e}{2}) \qquad N/m \tag{4.3}$$

Where $\rho_m = 3.3 \times 10^3\ Kg/m^3$ is the density of the asthenosphere, $\rho_w = 1 \times 10^3\ Kg/m^3$ density of the water, g = 9.8 m/s^2, $e = 3$ km is the elevation at the ridge and L = 8.5×10^4 m is the Plate thickness, for present day conditions. But, we are interested on the torque related to the Ridge Push force, which is the force times the radius of the earth, as follows

$$\vec{M}_{rp} = \vec{R} \times \left[ge(\rho_m - \rho_w)(\frac{L}{3} - \frac{e}{2})W_r\hat{n}\right] \qquad Nm \tag{4.4}$$

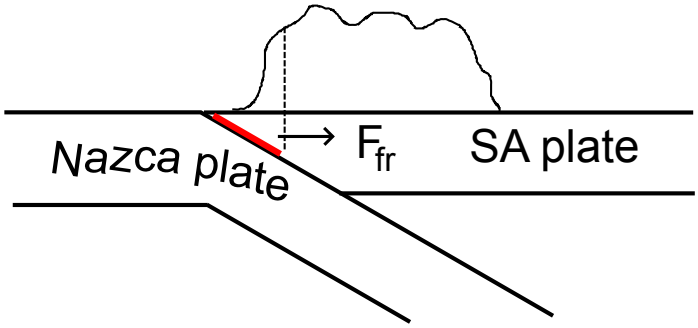

Figure 4.4: *Sketch of the friction force between the Nazca and South American plate. The red area represents the brittle zone.*

Where $\vec{R}$ is the distance from the centre of the Earth, $\hat{n}$ is the direction vector of the force and W_r is the length of the mid-ocean ridge in the South Atlantic region.

The magnitude of the ridge push torque for present day conditions is on the order of 7×10^{25} Nm. This force varies temporary with the elevation e of the mid-ocena ridge with respect to the rest of ocean floor. 70 Ma ago the elevation e of the ridge was 2 km giving a force variation on the order of a 30 % with respect to present day.

4.2 Forces that resist plate motions

The resisting forces are the ones that oppose the movement of the plate. Here we will review the friction force along the west margin of South America and the Andean forcing.

First, the frictional force along the South American trench, where it interacts with the Nazca plate.

$$\vec{F}_{fr} = fg\rho_c \frac{z^2}{2tan\theta} \qquad N/m$$

Where f is the frictional coefficient (depends on the thickness of the sediments at the trench), θ is the angle of subduction, z is the depth of 30 km to the end of the brittle zone, and $\rho_c = 2.8 \times 10^3$ Kg/m^3 is the density of the crust, see Fig. 4.4. The friction coefficient used was between 0.07 to 0.01 depending on the amount of sediments on the trench, the more sediments on the trench more lubricated is the subducting slab, reducing the friction coefficient. Frictional Torque,

$$\vec{M}_{fr} = \vec{R} \times \left[fg\rho_c \frac{z^2}{2tan\theta} W_t \hat{n} \right] \qquad Nm \tag{4.5}$$

Where W_t is the length of the trench and $\hat{n}$ is the direction of the force. The magnitude of this torque is 6×10^{25} Nm

The friction torque, described in equation 4.5, has two parameters that may vary temporary the friction coefficient and the slab geometry. However, the discussion about the friction coefficient is still

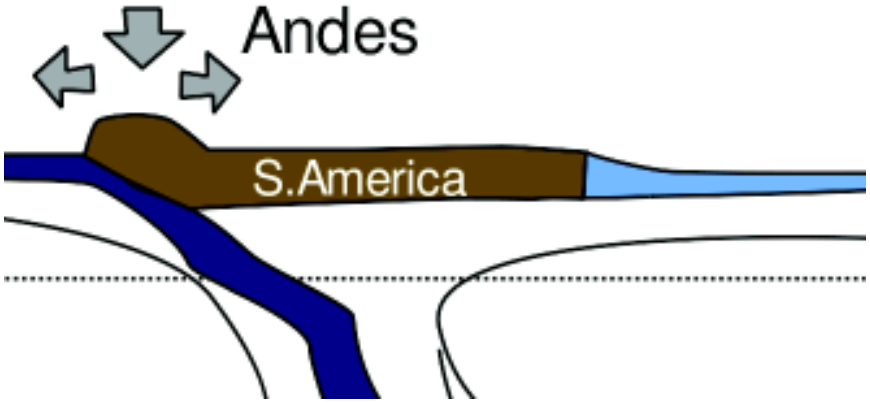

Figure 4.5: *Sketch of the Andean forcing.*

under debate, and additionally it is hard to constrain then for the past. In the case of the slab geometry its the same, because it is hard to know how much could it change during the past.

The magnitude of the Andean forcing done by the Andes for the present days was already estimated by Iaffaldano et al. in 2006 and is on the order of 1.4×10^{26} Nm. See Fig. 4.5 for a sketch of how vertical load of the topographic elevation of the Andes is balanced laterally. For what concerns on our calculations we are not interested in the magnitude of the Andean forcing in the past, but on the elevation of the Andes. Therefore, we will assume that the Andean force estimated by Iaffaldano et al. in 2006 only depends on the elevation of the Andes.

$$\vec{M}_{mb} = \zeta(h) \tag{4.6}$$

Where ζ is any function that depends only on the elevation h.

4.3 Flow velocity in the asthenosphere

At present day we can estimate three torques, the ridge push, Andean forcing and the friction force. It means that we can estimate the basal shear tractions necessary to maintain the balance on the system, see equation 4.1. However, for the basal shear equation 4.2 three parameters are unknown, the viscosity and thickness of the asthenospheric channel, and the flow velocity. To solve this problem, we will solve the torque balance equation 4.1 for a variety of combinations of viscosity and thickness of the channel. In order to obtain a viscosity-thickness-dependent flow velocity needed to maintain balance.

To start we separate the basal drag torque equation 4.2 in two components,

$$\begin{aligned}
\vec{M}_{bd} &= \int \vec{R}_d \times \frac{\mu}{D}\left((w_{ast} \times \vec{R}_b) - (w_{plate} \times \vec{R}_d)\right) dA \\
\vec{M}_{bd} &= \int \vec{R}_d \times \frac{\mu}{D}\left(w_{ast} \times \vec{R}_b\right) dA - \int \vec{R}_d \times \frac{\mu}{D}\left(w_{plate} \times \vec{R}_d\right) dA \\
\vec{M}_{bd} &= \vec{M}_{bd}^{ast} - \vec{M}_{bd}^{plate}
\end{aligned} \tag{4.7}$$

If we replace 4.7 in 4.1 and use 4.5, 4.4 and the value for the mountain building force estimated by Iaffaldano *et al.* (2006) 4.6 we get,

$$\begin{aligned}
\vec{M}_{fr} + \vec{M}_{mb} + \vec{M}_{rp} + \vec{M}_{bd}^{ast} - \vec{M}_{bd}^{plate} &= 0 \\
\vec{M}_{bd}^{ast} &= -\vec{M}_{fr} - \vec{M}_{mb} - \vec{M}_{rp} + \vec{M}_{bd}^{plate} \\
\vec{M}_{bd}^{ast} &= \vec{M}_t
\end{aligned} \tag{4.8}$$

The right hand side of equation 4.8 can be estimated from observations. The magnitudes of this forces are for $\vec{M}_{mb} = -1.4 \times 10^{26}\ Nm$, $\vec{M}_{fr} = -6 \times 10^{25}\ Nm$, $\vec{M}_{rp} = 7 \times 10^{25}\ Nm$ and $\vec{M}_{bd}^{plate} = 0.4 \times 10^{26}\ Nm$, thus the $\vec{M}_{bd}^{ast} = 1.7 \times 10^{26}\ Nm$. After some algebraic arrangement we can solve for $\vec{w}_{ast}$ using a linear system. $\vec{B}_{ij}$ is a matrix that comes out after solving $\vec{R} \times (\vec{w} \times \vec{R})$. Since $\vec{w}$ does not depend on the area and it can be taken outside of the integral.

$$\begin{aligned}
\int \vec{R}_d \times \frac{\mu}{D}\left(w_{ast} \times \vec{R}_b\right) dA &= \int \frac{\mu}{D} \vec{B}_{ij} \vec{w}_j dA \\
\vec{M}_{bd}^{ast} &= \underbrace{\int \frac{\mu}{D} \vec{B}_{ij} dA}_{\mathbf{G}_{ij}} \vec{w}_j
\end{aligned} \tag{4.9}$$

Comparing equation 4.8 and 4.9 we get,

$$\begin{aligned}
\mathbf{G}_{ij} \vec{w}_j &= \vec{M}_t \\
\vec{w}_j &= \mathbf{G}_{ij}^{-1} \vec{M}_t
\end{aligned} \tag{4.10}$$

As a result we obtain an asthenospheric flow velocity for a variety of combinations of flow viscosity and channel thickness (see table 4.1). The velocity obtained is proportional to the depth and inversely to the viscosity.

$$\vec{w} \sim \frac{D}{\mu}$$

	Channel thickness								
Flow viscosity	100 km	150 km	200 km	250 km	300 km	350 km	400 km	450 km	500 km
1×10^{18} Pa s	81.15	117.78	154.24	190.74	227.38	264.23	301.31	338.65	376.26
5×10^{18} Pa s	18.71	26.05	33.35	40.66	48.00	55.38	62.80	70.28	77.81
1×10^{19} Pa s	10.91	14.59	18.24	21.90	25.58	29.27	32.99	36.74	40.51
5×10^{19} Pa s	4.69	5.43	6.17	6.91	7.65	8.40	9.15	9.91	10.68
1×10^{20} Pa s	3.91	4.29	4.66	5.04	5.42	5.80	6.18	6.57	6.95

Table 4.1: Values of the flow velocity in asthenosphere in **cm per yr** for a variety of thickness and viscosity combinations. High flow velocities are related to low viscosity and thicker channel, while the low velocities are related to high viscosities and a thin channel.

The results in the table 4.1 displays several combinations of thickness and viscosity of the asthenospheric channel. It can be seen that the thicker the channel and the lower the viscosity, the faster is the flow velocity in the asthenosphere, up to 370 cm/yr. In the opposite case where the viscosity is high but the channel is thin, then the flow velocity in the asthenosphere is slow on the order of 4 cm/yr. For a fixed thickness, the lower the viscosity the faster the flow velocity in the asthenosphere, for a fix viscosity the thicker the channel the faster the flow velocity, this can be seen in the Fig. 4.6. We are interested in high flow velocities in the asthenosphere in order to drive plate motions.

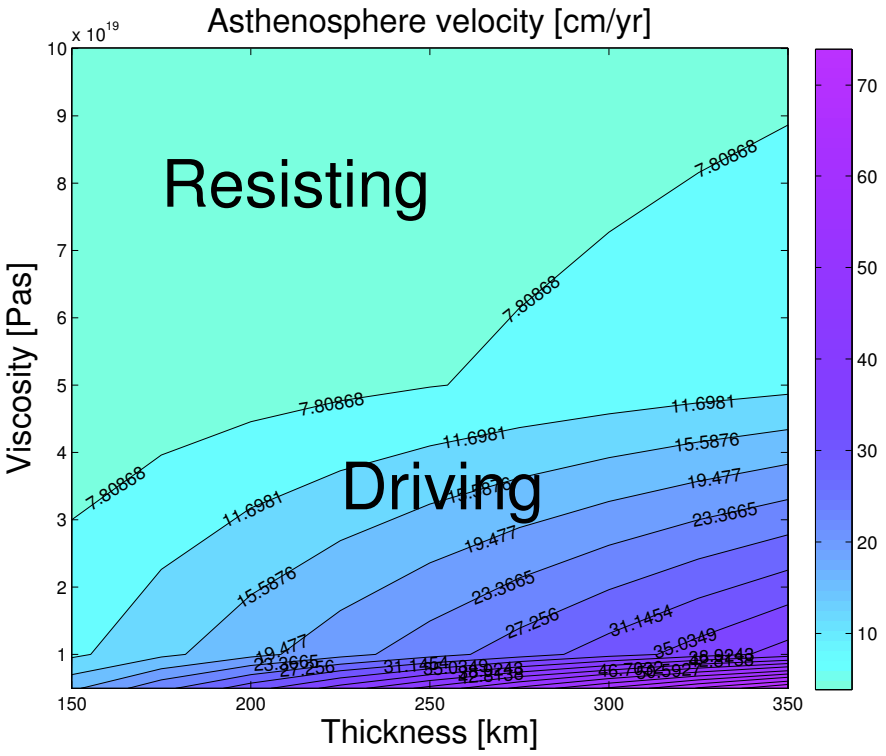

Figure 4.6: *Flow velocities in the asthenospheric channel. Flow velocities lower than the plate velocity make the basal shear tractions resist the movement instead of drive it. Higher velocities are related to a thicker channel and a low viscosity, while low velocities are related to thinner channel and high viscosity.*

Knowing the flow velocity in the asthenospheric channel and assuming it has not change trough time we have all the necessary parameters to estimate the Andean average elevation for past times, back to late Cretaceous (100 Ma). Our estimate of elevation, however, will depend on the combination of the viscosity and thickness of the channel, therefore our solution will be not unique.

4.4 Estimation of the average elevation of the Andes

In order to estimate the average topography for the Andes we have to go back to the torque balance 4.1. The four main forces acting on the South American plate are the friction, mountain weight, ridge push and basal drag. The calculations are going to be made between two time intervals, this means that we are not interested in the total forces but in their temporal variations, thereofre the forces that temporary varies comparatively little can be neglected. The next equation shows the time variation,

$$\vec{M}_{fr}^{t_1} + \vec{M}_{mb}^{t_1} + \vec{M}_{rp}^{t_1} + \vec{M}_{bd}^{t_1} = 0$$
$$\vec{M}_{fr}^{t_2} + \vec{M}_{mb}^{t_2} + \vec{M}_{rp}^{t_2} + \vec{M}_{bd}^{t_2} = 0$$

Since the order of magnitude of the ridge push and frictional forces are one order lower and their temporal variations are no more than a 30% in the case of the ridge push and for the frictional forces the temporal variation are complicated and not clear that to assume their constant or infer some variations its almost the same, in the sense of uncertainties. We can assume that both forces vary significantly little with time and for simplicity of the problem their temporal changes can be neglected. That makes $\vec{M}_{rp}^{t_2} - \vec{M}_{rp}^{t_1} = 0$ y $\vec{M}_{fr}^{t_2} - \vec{M}_{fr}^{t_1} = 0$. As a consequence we obtain,

$$\Delta\vec{M}_{mb} + \Delta\vec{M}_{bd} = 0 \tag{4.11}$$

According to equation 4.11 we can estimate the average elevation for past times, just balancing the Andean forcing with the basal shear tractions, as the latter can be calculated for the past, because it temporary depends on the observed plate velocity and the area of the plate, both know (see eq 4.2). Important to remember is that, in the M_{mb} the average elevation is the only parameter that varies temporary. The purpose is to obtain an average elevation relative to the present. The simplest way to do it, is given by the next relation.

$$\begin{aligned} \Delta\vec{M}_{mb} &= \Delta\vec{M}_{bd} \\ p &= \frac{\vec{M}_{mb}^{time}}{\vec{M}_{mb}^{present}} \qquad time = [present, ..., past] \end{aligned} \tag{4.12}$$

The basal drag equation 4.2 depends on the plate velocity, size of the South American plate (see Fig 4.7) and the flow velocity in the asthenosphere.

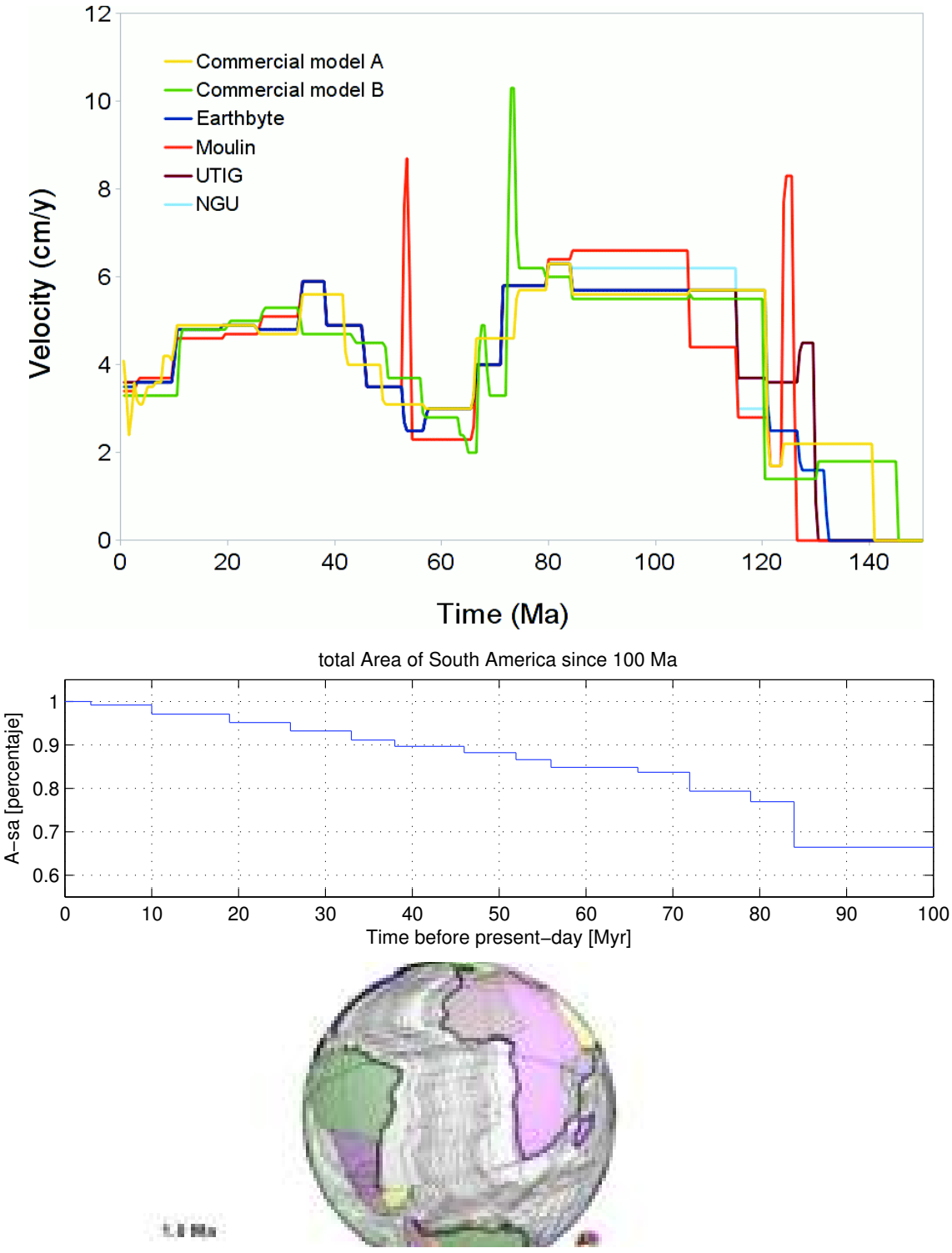

Figure 4.7: *Top, spreading rate velocity. Middle, area of the South American plate since late Cretaceous (100 Ma). Bottom, each grey line represent the contour of the plate area for an age, constrained from ocean floor age.*

Solving the torque balance between the basal shear tractions and the Andean forcing, using equation 4.11 and 4.12 results are as many as the data we have on the Table 4.1, it means 45 possible solutions. All of them are displayed on the chapter D.

Not all the solutions are plausible, we can discard directly the ones with a slow flow velocity in the asthenosphere (less than 7 cm/yr, see Fig. 4.6) and with too high flow velocity (more than 70 cm/yr), because they probability of that fast flow velocity in the asthenosphere is highly unreal. So, the range of solutions gets reduced by almost half. In the Fig. 4.8 are displayed all the solutions that are more plausible.

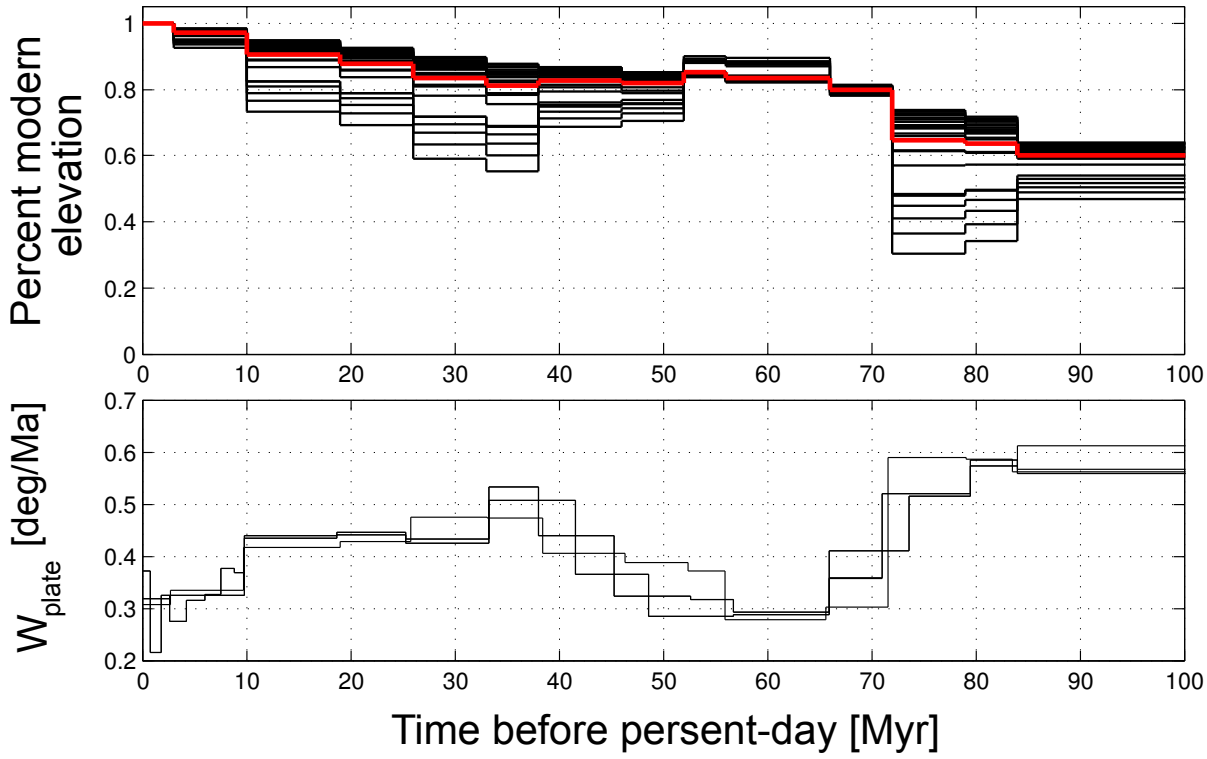

Figure 4.8: *Top: Average estimation of the Andean elevation with respect to present day topographic elevation, black lines are all the solutions and red line is the more reasonable solution (base on seismological data). Bottom: observed South American plate velocity. For both graphs the x-axis is the time. By 60 Ma all solutions show that the Andes have a high elevated topography (∼80 % of present day)*

The red line in the Fig. 4.8, is the more reasonable solution base on seismic data. In the Fig. 4.9 we can see that the Earth interior is segmented. The asthenosphere lays beneath the lithosphere and from the Fig. 4.9 right side, it can be restricted to a depth of 350 km to 410 km. The preferable viscosity value is on the order of 1×10^{19} Pa s as discussed by Hoeink and Lenardic (2008, 2010, 2011).

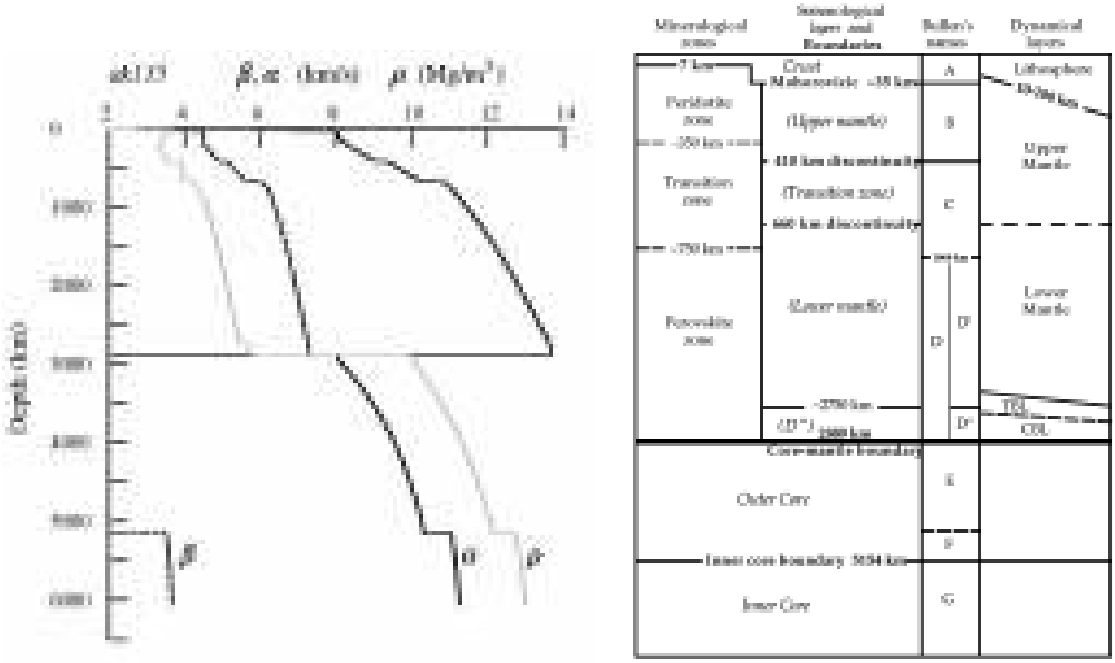

Figure 4.9: *Left:seismic structure of the Earth, α p-wave velocity, β s-wave velocity and ρ estimated Earth density. Right: Layers on the Earth interior, to our interest are the ones in the mantle (Davies, 1999).*

As discussed in the methodology, fast South American plate velocities are related to low elevation in the Andean topography, and vice versa. From 100 Ma to 70 Ma the elevation of the Andean topography was lower than by 60 Ma to 40 Ma, because prior 70 Ma the plate velocity was faster than after it. However all the solutions, showed in Fig. 4.8, exhibit that the elevation of the Andean topography was always relatively high, more than a 40 % by 70 Ma or later. This means that in order for the Andean orogenic history to explain the plate velocity variations, then the Andes should have been relatively high since 100 Ma.

Chapter 5

Discussion

Our force balance, as simple as it is, allows to understand key features in the relationship between boundary and basal shear forces. Boundary forces for the South American plate are well known. These are the ridge push, friction along the convergent margin and the tectonic force due to the Andean elevation. Basal shear force is related to pressure driven asthenospheric flow that drives South American plate motions. We assume a thin and low viscosity asthenosphere, with a time-independent constant flow velocity. Through the force balance we could show that the variations of the elevation of the Andean topography is not the main factor controlling plate motions, as other articles have suggested before (e.g., Husson & Ricard 2004, Norabuena *et al.* 1999). This was corroborated by revising the orogenic evolution of the Andes contributed by the geological record.

The elevation of the Andes, which is needed to explain the plate motion deceleration observed, according to our force balance, must have been on the order of 50 percent or higher in the past between 100 Ma to 60 Ma (e.g late Cretaceous to Paleocene). From the variety of results we have found the most suitable parameter values are a viscosity on the order of 10^{19} $Pa\ s$ and channel thickness of 250 km (350 km depth). When analysing the data with a channel thickness of 250 km and a viscosity of 1×10^{19} $Pa\ s$, our results displays that the elevation of the Andes by late Cretaceous and Paleocene (100 Ma to 60 Ma) were very high, no less than 60% of present day by late Cretaceous (100 Ma to 70 Ma) and up to 80% by Paleocene (60 Ma), see Fig. 5.1. This heigh elevated topography in the Andes resulting from our estimates, generates doubts.

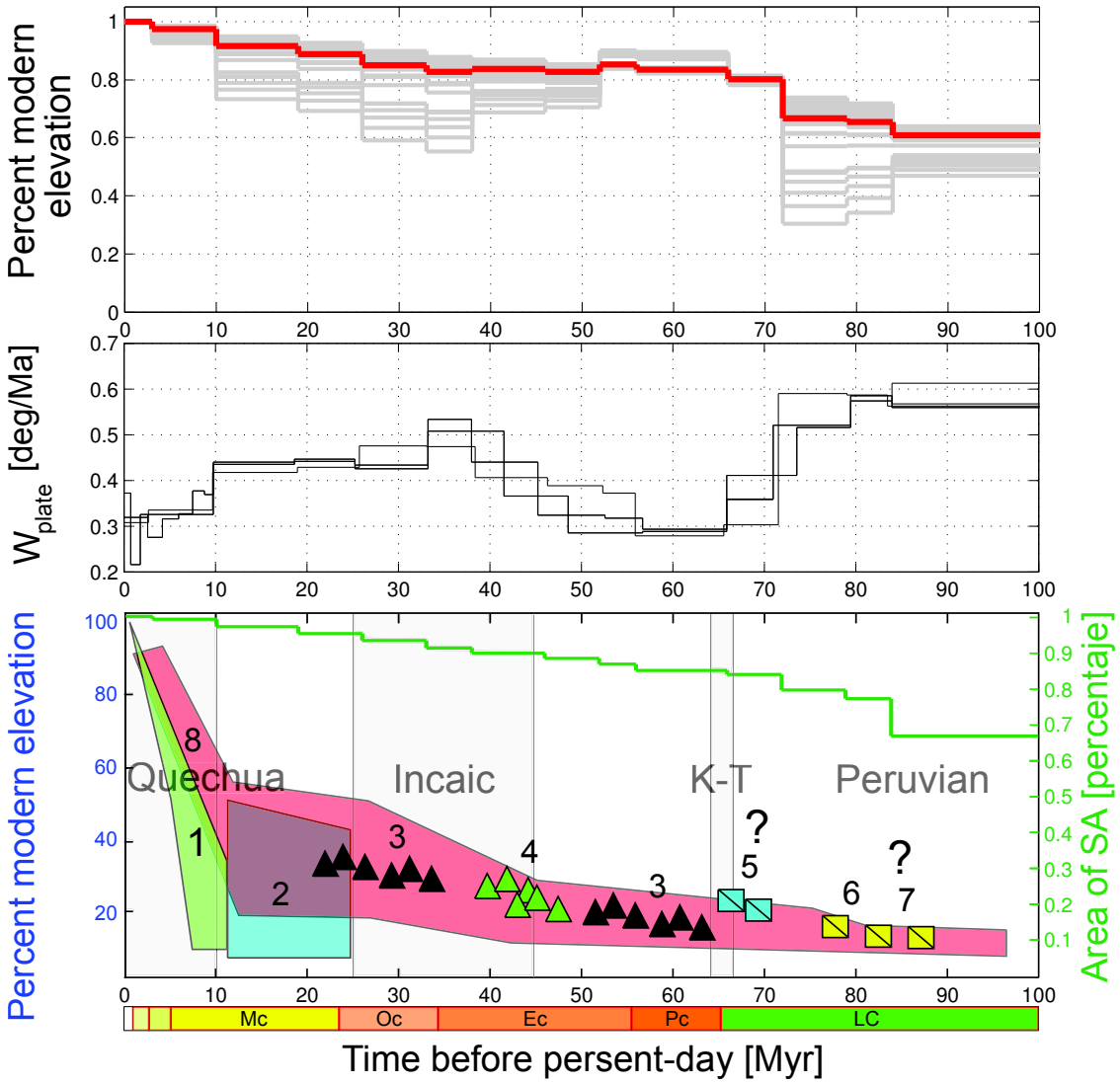

Figure 5.1: *Top: Estimate elevation of the Andean topography, red line in the more reasonable solution and in grey are the other solutions. Middle: Observed South American plate velocity. Bottom: Andean orogenic evolution since late Cretaceous. 1: oxygen isotopes is carbonates (Garzione* et al. *2006 and Ghosh* et al. *2006), 2: leaf morphology method in the Altiplano, Western and Eastern Cordillera (Gregory-Wodzicki, 2000), 3: AFT North Central Andes and Central Orocline (Hoorn* et al., *2010), 4: AFT in the Central Orocline (Gillis* et al., *2006), 5: unconformities in the Central Orocline (Cornejo* et al., *2003), 6: tectonic activity related to uplift in the Central Orocline (Sempere* et al., *1997), 7: tectonic activity related to uplift in the Northern Central Andes (Jaillard 1994 and Jaillard & Soler 1996), 8: Estimated Andean average elevation.*

The orogenic evolution of the Andes since late Cretaceous as inferred from the geological record, does not sustain the result of our force balance. The main periods of uplift in the Andes, where developed since middle Eocene (40 Ma) and presumably the elevation by Paleocene (60 Ma) and later was low.

During, late Cretaceous to Paleocene tectonic processes were active along the Andean margin, however no evidence exist of a high elevated Andes were present during that time period (e.g., Jaillard & Soler 1996, Sempere *et al.* 1997 among others). Moreover, the uplift presumably started slowly since middle Eocene, reaching a first peak of orogeny by late Oligocene and a second during late Miocene to present (e.g., Garzione *et al.* 2006 Gregory-Wodzicki 2000 Sempere *et al.* 1994 among others). According to this, the plate velocity variations cannot be explained by variations in the elevation of the Andean topography. Neither can this velocity changes be explained by a reduced size of the plate, see Fig 5.1 bottom green line, because it does not vary more than a 20 percent for past times. Changes in the flux of the asthenosphere can offer an alternative explanation.

The flux of the asthenosphere depends on the thickness and viscosity of the asthenospheric channel. We assumed a channel thickness of 250 km (as the more reasonable value) and considering a lithosphere thickness of 100 km, for a total depth of 350 km. This values could be mistaken. However, the values used for the thickness and viscosity of the channel can be corroborated by seismic tomography images, see Fig. 5.2. Seismic tomography allows to understand deep Earth structures. Mantle anisotropy are normally associated with the mantle flow direction, due to elongated crystalline structure. Thus, seismic tomography images in Figure 5.2 show low S-wave velocities related to a high material mobility (e.g., low viscosity on the order of 10^{19} Pa s), establishing that the bottom of the asthenospheric channel lies between 350 to 400 km depth, as can be deduced for the two seismic cross sections. Thus, seismic tomography agrees with the values we used for the channel thickness.

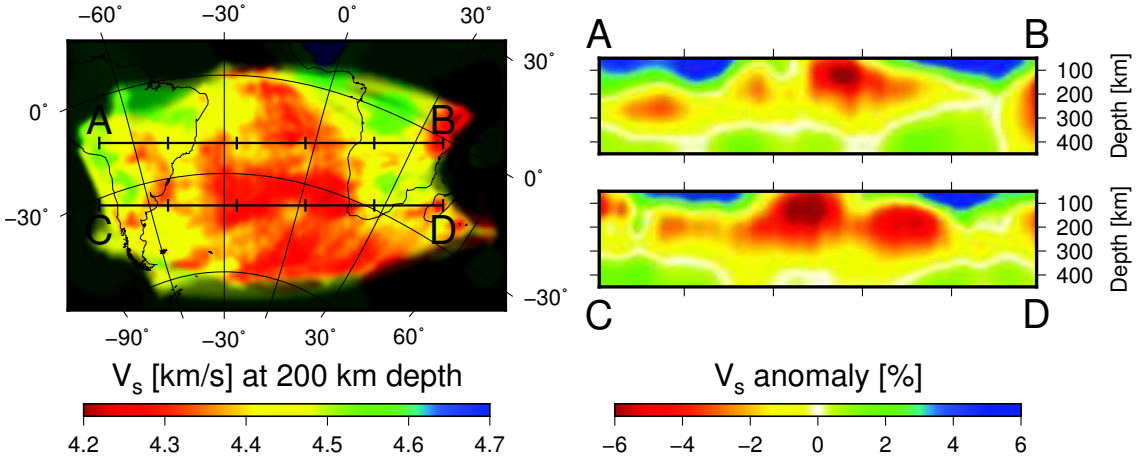

Figure 5.2: *Full waveform tomography image for the South Atlantic region. Left: 200 km depth seismic images for the South Atlantic. Right: Two vertical profiles(Colli* et al.*, 2012).*

The viscosity value used is corroborated by the geoid observation over the Earth. The geoid is defined as the equipotential surface of the gravity field that is coincident with the surface of the oceans. It is useful because it is more sensitive than gravity to deeper or larger-scale density variations. In the image of the South America region, see Fig. 5.3, the warm coloured zone represents the high density material flowing downward. Flowing material in the asthenosphere has to go down. Through this the geoid reveals a thickness of this downward channel of rough $\sim$ 2000 km that is the wide of the red zone over South

America, estimated from Fig. 5.3. Now the flow velocity in the asthenosphere is 10^1 cm/yr for a 250 km, compared to the $\sim$ 2000 km thick downward channel, then the velocity downward results on the order of 1 cm/yr. In Earth mantle, velocities decrees in depth depending on a logarithmic scale to the viscosity (Gurnis & Davies, 1986). In the lower mantle average viscosities are on the order of 10^{23} $Pa\ s$ (Mitrovica & Forte, 2004). Having a flow velocity in the asthenosphere on the order of 10^1 cm/yr with a viscosity of 10^{19} $Pa\ s$, results in a viscosity contrast is 10^4 $Pa\ s$ and $ln(10^4) \approx 10$, leading to velocities in the lower mantle on the order of 1 cm/yr. This two methods result in velocities for the deeper mantle on the order of 1 cm/yr, which are congruent with the values chosen for the thickness and viscosity of the asthenospheric channel. Deep mantle flow velocities are on the order of 1 cm/yr (Bunge *et al.* 1998 and Gurnis & Davies 1986) Further, low viscosity asthenosphere promotes long wavelength of mantle flow (Bunge *et al.*, 1998).

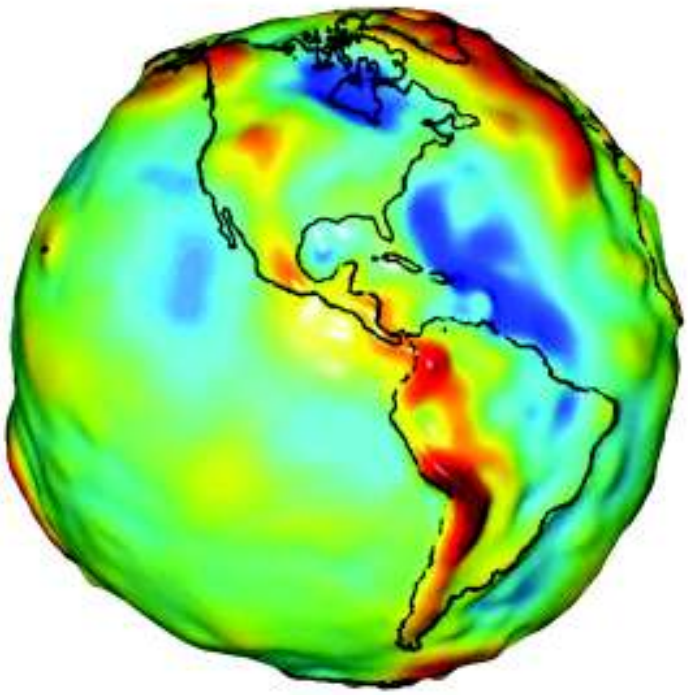

Figure 5.3: *Geoid image for the South American region. Warm colour regions are related to high density zones, while cold colour regions are related to lower density zones.*

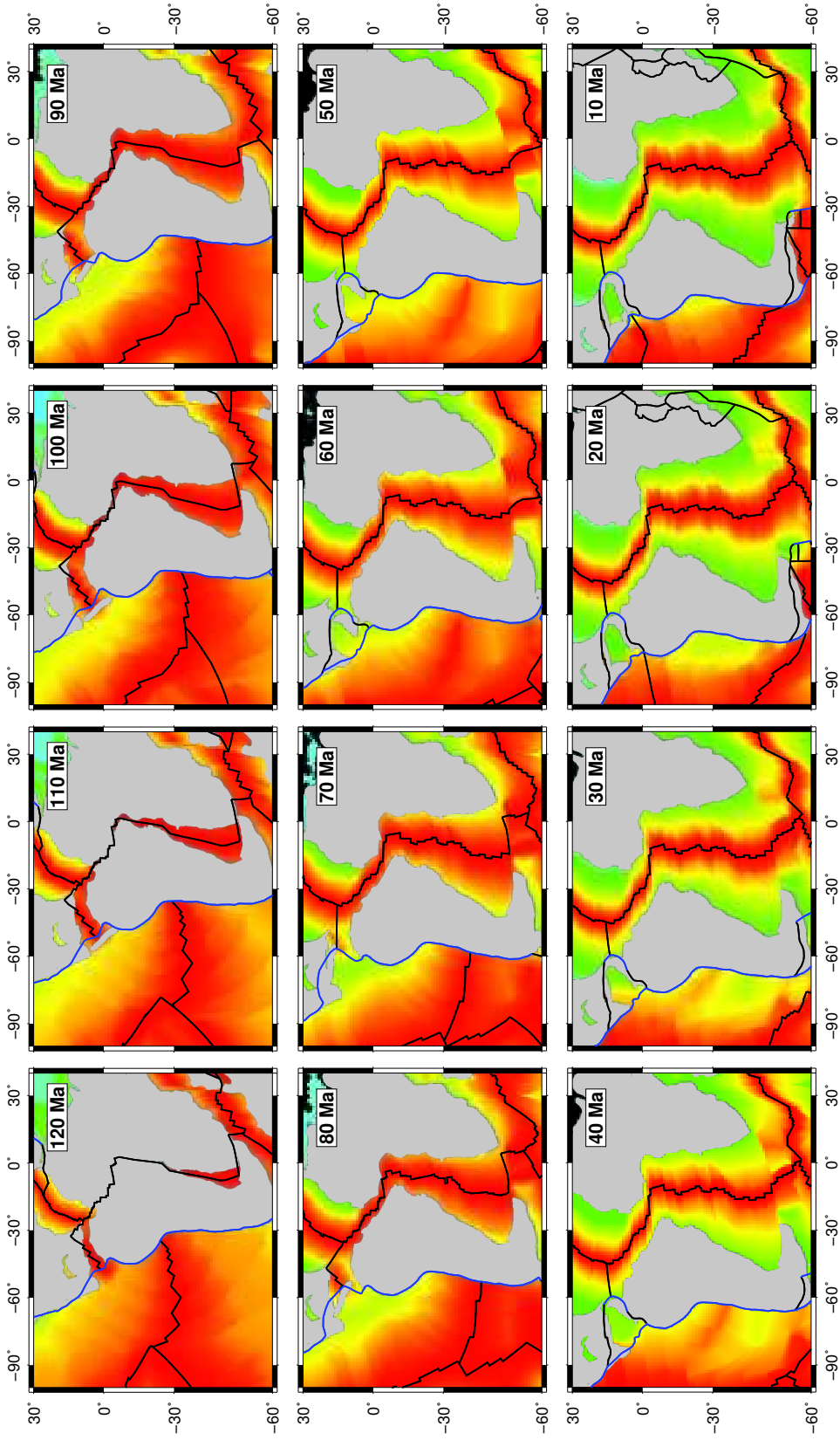

Figure 5.4: *Evolution of the Plate configuration since late Cretaceous (120 Ma). It the figure can be appreciated that Africa has remain almost in the same place, whereas the South American continent has moved westward and how has evolved the plates in the side of the Pacific (e.g., Farallon, Phoenix and Nazca plates) (Müller et al., 2008b).*

The evolution on the plate configuration has undergone important changes since late Cretaceous (100 Ma) to present, as can be seen in the Figure 5.4. The more out standing change is at $\sim$ 60 Ma when the Aluk ridge, in front of the South American plate, stopped and migrated far South. Previous to its migration, the ridge was allowing material to go from the South Atlantic region in to the Pacific region. Thus, after his close no more material was allowed to cross into the Pacific region. This correlates with the K-T event described in the geology by $\sim$ 60 Ma, see Fig. 5.1. The new plate configuration allow to the asthenosphere flux to push the trench westward, accelerating the South American plate.

In the Fig. 5.4 can be seen how the configuration of the plates (e.g., Farallon/Nazca) has change since 100 Ma. This makes hard to believe the assumption that the friction forces is constant through time. However, the assumption taken was for simplification of the problem, its is undoubtedly that the friction force was different in the past. But, how different was it? was it lower or higher? this questions are almost impossible to answer, besides the friction coefficient between the overriding and subducting plate is not well constrained and understood. Therefore, the assumption on leaving the frictional force constant through time was the simplest and smartest option.

Flow velocity changes in the asthenosphere are affected by pressure driven mechanism connected to lateral variation on the surface topography. The asthenosphere flow beneath the South Atlantic can be described by a pressure driven Poiseuille flux (Hoeink *et al.*, 2011). For this to be true, topography signals on the plate have must be present. Japsen *et al.* (2012) described epeirogenic uplift periods in the north east Brazil, specifically during late Cretaceous (80 Ma), Eocene (40 Ma) and Miocene (15 Ma). These periods of uplift correlates with the orogenic evolution of the Andes (Steinmann *et al.*, 1929). Further, the African Superswell is characterized by dynamically supported topography (Nyblade & Robinson, 1994), with an estimated elevation of rough $\sim 1\ km$ in contrast to the conjugate South American plate, that corresponds the difference between the Argentine basin in South America with the Cape Basin in Africa, see Fig. 1.4. Janssen *et al.* (1995) argued a temporal and spatial correlation between phase of subsidence in African basins and variations in plate motions during tertiary. Furthermore, Burke & Gunnell (2008) described that Africa started to be flexed upward when the Afar plume erupted ca. 31 Ma. The pronounced dynamic topography gradient across the South Atlantic region, implies significant westward flow in the asthenosphere, as suggested by Behn *et al.* (2004).

$$\vec{v} \quad = \quad -\frac{h^2}{8\eta}\frac{\Delta P}{\Delta x} \tag{5.1}$$

To assess the dynamical feasibility of westward fluxing asthenosphere across the South Atlantic region from a simple fluid dynamic model for pressure driven flow in a low viscosity channel, where the asthenosphere channel is approximated as a viscous fluid confined between two fixed, horizontal infinite planes separated by a distance h. The excess of velocity due to the horizontal pressure gradient $\frac{\Delta P}{\Delta x}$ that arises in the channel varies parabolically with depth, see equation 5.1. Thus, taking $\sim 1\ km$ of topography difference over a distance of 7000 km, leads to a pressure gradient of 300 $bars$ and assuming an asthenosphere viscosity of $1 \times 10^{19}\ Pas$ and a channel thickness 250 km, this yields to a velocity of $\sim 10\ cm/yr$. This results is on the same order of magnitude as the estimation for the flow velocity in the asthenosphere in order to maintain balance with present day boundary forces.

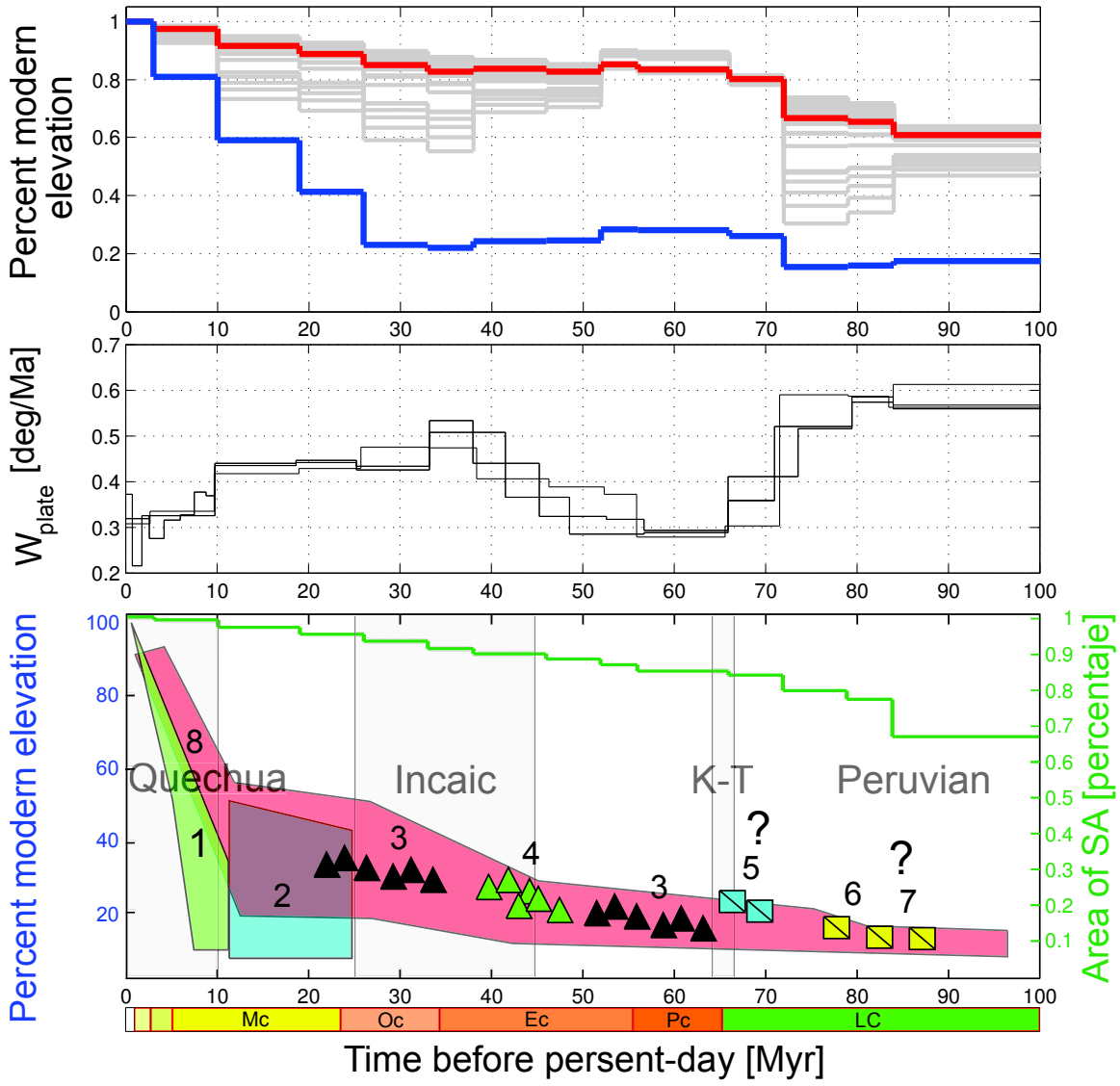

Figure 5.5: *Top: Estimate elevation of the Andean topography, red line is the more reasonable solution and in grey are the other solutions and blue line is the new estimation of the elevation of the Andes considering a pressure driven (Poiseuille) flux from Africa to South America. Middle: Observed South American plate velocity. Bottom: Andean orogenic evolution since late Cretaceous. 1: oxygen isotopes is carbonates (Garzione* et al. *2006 and Ghosh* et al. *2006), 2: leaf morphology method in the Altiplano, Western and Eastern Cordillera (Gregory-Wodzicki, 2000), 3: AFT North Central Andes and Central Orocline (Hoorn* et al., *2010), 4: AFT in the Central Orocline (Gillis* et al., *2006), 5: unconformities in the Central Orocline (Cornejo* et al., *2003), 6: tectonic activity related to uplift in the Central Orocline (Sempere* et al., *1997), 7: tectonic activity related to uplift in the Northern Central Andes (Jaillard 1994 and Jaillard & Soler 1996), 8: Estimated Andean average elevation.*

Repeating the calculations done previously, but this time taking into account a contribution on the flux in the asthenosphere due to a pressure driven (Poiseuille) flow from the African into the South American plate since early Oligocene (35 Ma) (Burke & Gunnell, 2008). The new results displayed in the Fig. 5.5 blue line match in an excellent manner with the geological information.

Thus, dynamic topography variations plays a important role in plate motions, through a thin low viscosity asthenosphere influenced by pressure gradients. Our novel approach contributes to a more integral understanding of plate motion, not only due to boundary forces, but also by basal shear forces and the influence of dynamic topography.

Chapter 6

Conclusion

By simple calculations of a force balance between the boundary and the basal shear forces, temporal plate motions variations can be explained. South American plate motions describes a velocity decrease in late Cretaceous (70 Ma) follow by a speed up and a final deceleration since early Oligocene (35 Ma). This is the first time that somebody has try to explain plate motions for a long time period 100 Ma. Our assumption is base on that plate motions are driven by basal shear forces related to pressure driven (Poiseuille) low viscosity asthenosphere flow beneath the lithosphere. Boundary forces cannot fully explain plate motions, because high elevation on the Andean topography will be needed for past times in order to explain the velocity decelerations. The geological record of the Andes has shown that the more prominent uplift phases occurred since the middle Eocene (40 Ma). Our assumption on a thin asthenospheric layer is tested by comparing it with full waveform seismic topography images, thus validating our choice on the more reasonable solutions. We used the geoid observation, accompanied by convection studies (Gurnis & Davies, 1986), to test the feasibility of a low viscosity asthenosphere. Further, a low viscosity asthenosphere promotes long wavelength mantle circulation (Bunge *et al.*, 1998). Pressure gradients affects asthenospheric flow velocities, due to lateral topographic variations (e.g., Dynamic topography). The African plateau has experienced several epeirogenic changes during the tertiary, that are in temporal and spatially correlation with South American plate motions. The pronounced dynamic topography gradient across the South Atlantic region, implies significant westward flow in the asthenosphere. This hypothesis is tested by assuming a pressure driven (Poiseuille) flow in the asthenosphere, resulting in flow velocity magnitude on the order of 10 cm/yr, due to pressure gradients of 300 $bars$, done by a topography contrast of 1 km. Repeating the calculation on the estimation of the elevation of the Andean topography, but considering the contribution of a pressure driven flow from Africa to South America, results are in better correlation with the geological evolution of the Andes.

We have reviewed forces that acts on the South American plate, but also have accounted for all the other external aspects that can play a role into affecting South American plate motions, such as dynamic topography and the plate configuration on the Pacific side. As a matter of fact, this work is the first one attempting to explain plate velocity variations for a long time period (100 Ma), integrating simple but robust mechanism. Our novel approach contributes to a more integral understanding of plate motion, not only due to boundary forces, but also by basal shear forces and the influence of far field effects, such

as dynamic topography in the adjacent plates.

Bibliography

Amante, C. & Eakins, B. W. (2009). ETOPO1 Arc-Minute Global Relief Model: Procedures, Data Sources and Analysis .

Anderson, D. L. (1982). Hotspots, polar wander, Mesozoic convection and the geoid. *Nature* **297**, 391–393.

Aragon, E., Goin, F. J., Aguilera, Y. E., Woodburne, M. O., Carlini, A. A. & Roggiero, M. F. (2011). Palaeogeography and palaeoenvironments of northern Patagonia from the late Cretaceous to the Miocene: the Palaeogene Andean gap and the rise of the North Patagonian High Plateau. *Biological Journal of the Linnean Society* **103**(2), 305–315.

Arriagada, C., Roperch, P., Mpodozis, C. & Cobbold, P. R. (2008). Paleogene building of the Bolivian orocline: Tectonic restoration of the central andes in 2-d map view. *Tectonics* **27**(6).

Barke, R. & Lamb, S. (2006). Late cenozoic uplift of the eastern cordillera, bolivian andes. *Earth and Planetary Science Letters* **249**(3-4), 350–367.

Barnes, J., Ehlers, T., McQuarrie, N., O'Sullivan, P. & Pelletier, J. (2006). Eocene to recent variations in erosion across the central Andean fold-thrust belt, northern Bolivia: Implications for plateau evolution. *Earth and Planetary Science Letters* **248**(1–2), 118 – 133. URL http://www.sciencedirect.com/science/article/pii/S0012821X06003712.

Behn, M., Conrad, C. & Silver, P. (2004). Detection of upper mantle flow associated with the african superplume. *Earth and Planetary Science Letters* **224**(3-4), 259–274.

Bianchi, M. C., Sabadini, R. & Bunge, H.-P. (2011). Analysing the variations in plate motions in the south Atlantic. *Universita' degli studi di Milano* Master's thesis.

Buck, W. R., Small, C. & Ryan, W. B. F. (2009). Constraints on asthenospheric flow from the depths of oceanic spreading centers: The east pacific rise and the australian-antarctic discordance. *Geochemistry Geophysics Geosystems* **10**.

Bullard, E., Everett, J. E. & Smith, A. G. (1965). The fit of the continents around the atlantic. *Philosophical Transactions of the Royal Society of London. Series A, Mathematical and Physical Sciences* **258**(1088), 41–51. A Symposium on Continental Drift.

Bunge, H., Ricard, Y. & Matas, J. (2001). Non-adiabaticity in mantle convection. *Geophysical Research Letters* **28**(5), 879–882.

Bunge, H., Richards, M. & Baumgardner, J. (1996). Effect of depth-dependent viscosity on the planform of mantle convection. *Nature* **379**(6564), 436–438.

Bunge, H., Richards, M., Lithgow-Bertelloni, C., Baumgardner, J., Grand, S. & Romanowicz, B. (1998). Time scales and heterogeneous structure in geodynamic earth models. *Science* **280**(5360), 91–95.

Burke, K. & Gunnell, Y. (2008). The african erosion surface: A continental-scale synthesis of geomorphology, tectonics, and environmental change over the past 180 million years. *The Geological Society of America, Memoirs* **201**, 21.

Cande, S., Labrecque, J. & Haxby, W. (1988). Plate kinematics of the south-atlantic-chron c34 to present. *Journal of Geophysical Research-Solid Earth and Planets* **93**(B11), 13479–13492.

Charrier, R., Pinto, L. & Rodriguez, M. P. (2007). Tectonostratigraphic evolution of the Andean orogen in Chile. *The Geology of Chile, The Geological Society of London* , 221.

Cobbold, P. & Rossello, E. (2003). Aptian to recent compressional deformation, foothills of the Neuquén basin, Argentina. *Marine and Petroleum Geology* **20**(5), 429 – 443. URL http://www.sciencedirect.com/science/article/pii/S0264817203000771.

Colli, L., Fichtner, A. & Bunge, H.-P. (2012). Full waveform tomography of the upper mantle in the South Atlantic region: evidence for pressure-driven westward flow in a shallow asthenosphere. *Tectonophysics* In press.

Cornejo, P., Matthews, S. & de Arce, C. P. (2003). The K-T compressive deformation event in northern Chile 24-27 s. *10 Geological Congress in Concepcion Chile* .

Crosby, A. G., McKenzie, D. & Sclater, J. G. (2006). The relationship between depth, age and gravity in the oceans. *Geophys. J. Int.* **166**(2), 553–573.

Davies, G. (1988). Ocean bathymetry and mantle convection large-scale flow and hotspots. *Journal of Geophysical Research-Solid Earth and Planets* **93**(B9), 10467–10480.

Davies, G. F. (1999). *Dynamic Earth: Plates, Plumes and Mantle Convection*. Cambridge, First Edition ed.

Debayle, E., Kennett, B. & Priestley, K. (2005). Global azimuthal seismic anisotropy and the unique plate-motion deformation of australia. *Nature* **433**(7025), 509–512.

Ege, H., Sobel, E. R., Scheuber, E. & Jacobshagen, V. (2007). Exhumation history of the southern altiplano plateau (southern bolivia) constrained by apatite fission track thermochronology. *Tectonics* **26**(1).

Farías, R., M., Charrier, S., Carretier, J., Martinod, A., Fock, D., Campbell, J., Cáceres & Comte, D. (2008). Late miocene high and rapid surface uplift and its erosional response in the Andes of central Chile (33–35 s). *Tectonics* **27**.

Folguera, A., Orts, D., Spagnuolo, M., Rojas Vera, E., Litvak, V., Sagripanti, L., Ramos, M. E. & Ramos, V. A. (2011). A review of Late Cretaceous to Quaternary palaeogeography of the southern andes. *Biological Journal of the Linnean Society* **103**(2), 250–268.

Fowler, C. (2009). *The Solid Earth: An Introduction to Global Geophysics*. Cambridge, Second Edition ed.

Gansser, A. (1973). Factsand theories on the andes. *Journal of the Geological Society of London.* (129), 93–131.

Garzione, C. N., Molnar, P., Libarkin, J. C. & MacFadden, B. J. (2006). Rapid late Miocene rise of the Bolivian Altiplano: Evidence for removal of mantle lithosphere. *Earth and Planetary Science Letters* **241**(3–4), 543 – 556.

Ghosh, P., Garzione, C. & Eiler, J. (2006). Rapid uplift of the altiplano revealed through c-13-o-18 bonds in paleosol carbonates. *Science* **311**(5760), 511–515.

Gillis, R. J., Horton, B. K. & Grove, M. (2006). Thermochronology, geochronology, and upper crustal structure of the cordillera real: Implications for cenozoic exhumation of the central andean plateau. *Tectonics* **25**(6).

Gregory-Wodzicki, K. (2000). Uplift history of the central and northern Andes: A review. *Geological Society of America Bulletin* **112**(7), 1091–1105.

Gurnis, M. & Davies, G. (1986). Mixing in numerical models of mantle convection incorporating plate kinematics. *Journal of Geophysical Research* **6**, 375–395.

Hager, B. & Richards, M. (1989). Long-wavelength variations in earths geoid - physical models and dynamical implications. *Philosophical Transactions of the Royal Society of London Series A-Mathematical Physical and Engineering Science* **328**(1599), 309–327.

Hartley, A. (2003). Andean uplift and climate change. *Journal of the Geological Society* **160**(Part 1), 7–10.

Hartley, A. J., Sempere, T. & Woerner, G. (2007). A comment on rapid late miocene rise of the Bolivian Altiplano: Evidence for removal of mantle lithosphere by C.N. Garzione et al. Earth Planet. sci. lett. 241 (2006) 543-556. *Earth and Planetary Science Letters* **259**(3-4), 625–629.

Hoeink, T., Jellinek, A. M. & Lenardic, A. (2011). Viscous coupling at the lithosphere-asthenosphere boundary. *Geochemistry Geophysics Geosystems* **12**.

Hoeink, T. & Lenardic, A. (2008). Three-dimensional mantle convection simulations with a low-viscosity asthenosphere and the relationship between heat flow and the horizontal length scale of convection. *Geophysical Research Letters* **35**(10).

Hoeink, T. & Lenardic, A. (2010). Long wavelength convection, poiseuille-couette flow in the low-viscosity asthenosphere and the strength of plate margins. *Geophysical Journal International* **180**(1), 23–33.

Hoeink, T., Lenardic, A. & Richards, M. (2012). Depth-dependent viscosity and mantle stress amplification: implications for the role of the asthenosphere in maintaining plate tectonics. *Geophysical Journal International* **191**(1), 30–41.

Hoorn, C., Wesselingh, F. P., ter Steege, H., Bermudez, M. A., Mora, A., Sevink, J., Sanmartin, I., Sanchez-Meseguer, A., Anderson, C. L., Figueiredo, J. P., Jaramillo, C., Riff, D., Negri, F. R., Hooghiemstra, H., Lundberg, J., Stadler, T., Saerkinen, T. & Antonelli, A. (2010). Amazonia through time: Andean uplift, climate change, landscape evolution, and biodiversity. *Science* **330**(6006), 927–931.

Horton, B. (2005). Revised deformation history of the central Andes: Inferences from Cenozoic foredeep and intermontane basins of the Eastern cordillera, Bolivia. *Tectonics* **24**(3).

Husson, L., Conrad, C. P. & Faccenna, C. (2012). Plate motions, Andean orogeny, and volcanism above the South Atlantic convection cell. *Earth and Planetary Science Letters* **317**, 126–135.

Husson, L. & Ricard, Y. (2004). Stress balance above subduction: application to the andes. *Earth and Planetary Science Letters* **222**(3-4), 1037–1050.

Iaffaldano, G., Bunge, H.-P. & Dixon, T. H. (2006). Feedback between mountain belt growth and plate convergence. *Geology* **34**(10), 893–896.

Jaillard, E. (1994). Kimmeridgian to Paleocene tectonic and geodynamic evolution of the Peruvian (and Ecuadorian) margin. In: *Cretaceous tectonics of the Andes*, Earth Evolution Sciences. Vieweg, pp. 101–167. URL http://www.documentation.ird.fr/hor/fdi:010019764.

Jaillard, E., Cappertta, H., Ellenberger, P. & Feist, M. (1993). Sedimentology, paleontology, biostratigraphy and correlation of the late Cretaceous vilquenchico group of southern Peru. *Cretaceous Research* **14**(6), 623–661.

Jaillard, E. & Soler, P. (1996). Cretaceous to early Paleogene tectonic evolution of the northern central Andes (0-18 s) and its relations to geodynamics. *Tectonophysics* **259**(1-3), 41–53.

Janssen, M., Stephenson, R. & Cloetingh, S. (1995). Temporal and spatial correlations between changes in plate motions and the evolution of rifted basins in Africa. *Geological Society of America Bulletin* **107**(11), 1317–1332.

Japsen, P., Bonow, J. M., Green, P. F., Cobbold, P. R., Chiossi, D., Lilletveit, R., Magnavita, L. P. & Pedreira, A. (2012). Episodic burial and exhumation in ne brazil after opening of the south atlantic. *Geological Society of America Bulletin* **124**(5-6), 800–816.

Karato, S. & Jung, H. (1998). Water, partial melting and the origin of the seismic low velocity and high attenuation zone in the upper mantle. *Earth and Planetary Science Letters* **157**(3-4), 193–207.

McQuarrie, N., Barnes, J. B. & Ehlers, T. A. (2008). Geometric, kinematic, and erosional history of the central Andean plateau, Bolivia (15-17 s). *Tectonics* **27**(3).

Mitrovica, J. & Forte, A. (2004). A new inference of mantle viscosity based upon joint inversion of convection and glacial isostatic adjustment data. *Earth and Planetary Science Letters* **225**(1-2), 177–189.

Morgan, J., Morgan, W., Zhang, Y. & Smith, W. (1995). Observational hints for a plume-fed,suboceanic asthenosphere and its role in mantle convection. *Journal of Geophysical Research-Solid Earth* **100**(B7), 12753–12767.

Mpodozis, C., Arriagada, C., Basso, M., Roperch, P., Cobbold, P. & Reich, M. (2005). Late mesozoic to paleogene stratigraphy of the salar de atacama basin, antofagasta, northern chile: Implications for the tectonic evolution of the central andes. *Tectonophysics* **399**(1-4, SI).

Müller, R., Roest, W., Royer, J., Gahagan, L. & Sclater, J. (1997). Digital isochrons of the world's ocean floor. *Journal of Geophysical Research-Solid Earth* **102**(B2), 3211–3214.

Müller, R. D., Sdrolias, M., Gaina, C. & Roest, W. R. (2008a). Age, spreading rates, and spreading asymmetry of the world's ocean crust. *Geochem. Geophy. Geosy.* **9**(4).

Müller, R. D., Sdrolias, M., Gaina, C. & Roest, W. R. (2008b). Age, spreading rates, and spreading asymmetry of the world's ocean crust. *Geochemistry Geophysics Geosystems* **9**.

Norabuena, E., Dixon, T., Stein, S. & Harrison, C. (1999). Decelerating nazca-south america and nazca-pacific plate motions. *Geophysical Research Letters* **26**(22), 3405–3408.

Nurnberg, D. & Müller, R. (1991). The tectonic evolution of the south-atlantic from late Jurassic to present. *Tectonophysics* **191**(1-2), 27–53.

Nyblade, A. & Robinson, S. (1994). The african superswell. *Geophysical Research Letters* **21**(9), 765–768.

Picard, D., Sempere, T. & Plantard, O. (2008). Direction and timing of uplift propagation in the Peruvian Andes deduced from molecular phylogenetics of highland biotaxa. *Earth and Planetary Science Letters* **271**(1–4), 326 – 336. URL http://www.sciencedirect.com/science/article/pii/S0012821X08002628.

Rapela, C., Pankhurst, R., Casquet, C., Baldo, E., Saavedra, J. & Galindo, C. (1998). Early evolution of the Proto-Andean margin of South America. *Geology* **26**(8), 707–710.

Schuberth, B. S. A., Bunge, H. P. & Ritsema, J. (2009). Tomographic filtering of high-resolution mantle circulation models: Can seismic heterogeneity be explained by temperature alone? *Geochemistry Geophysics Geosystems* **10**.

Sempere, T., Butler, R., Richards, D., Marshall, L., Sharp, W. & Swisher, C. (1997). Stratigraphy and chronology of upper cretaceous lower paleogene strata in bolivia and northwest argentina. *Geological Society of America Bulletin* **109**(6), 709–727.

Sempere, T., Folguera, A. & Gerbault, M. (2008). New insights into andean evolution: An introduction to contributions from the 6th isag symposium (barcelona, 2005). *Tectonophysics, in the press* .

Sempere, T., Hartley, A. & Roperch, P. (2006). Comment on "rapid uplift of the altiplano revealed through c-13-o-18 bonds in paleosol carbonates. *Science* **314**(5800).

Sempere, T., Herail, G., Oller, J. & Bonhonmme, M. (1990). Late Oligecene early Miocene major tectonic crisis and related basins in Bolivia. *Geology* **18**(10), 946–949.

Sempere, T., Marshall, L., Rivano, S. & Godoy, E. (1994). Late Oligocene early Miocene compresional tectosedimentary episode and associated land-mammal faunas in the Andes of central Chile and adjacent Argentina (32-37 s). *Tectonophysics* **229**(3-4), 251–264.

Simmons, N. & Grand, S. (2002). Partial melting in the deepest mantle. *Geophysical Research Letters* **29**(11).

Simmons, N. A., Forte, A. M. & Grand, S. P. (2007). Thermochemical structure and dynamics of the african superplume. *Geophysical Research Letters* **34**(2).

Steinmann, G., Lisson, C. I., Sieberg, A. & Stappenbeck, R. (1929). Geologie von Peru .

Tassara, A. & Yanez, G. (2003). Relationship between elastic thickness and the tectonic segmentation of the Andean margin. *Revista Geologica de Chile* **30**(2), 159–186.

Thomson, S. (2002). Late cenozoic geomorphic and tectonic evolution of the patagonian andes between latitudes 42 degrees s and 46 degrees s: An appraisal based on fission-track results from the transpressional intra-arc liquine-ofqui fault zone. *Geological Society of America Bulletin* **114**(9), 1159–1173.

Tkalcic, H. & Romanowicz, B. (2002). Short scale heterogeneity in the lowermost mantle: insights from pcp-p and scs-s data. *Earth and Planetary Science Letters* **201**(1), 57–68.

Tunik, M., Folguera, A., Naipauer, M., Pimentel, M. & Ramos, V. A. (2010). Early uplift and orogenic deformation in the Neuquén basin: Constraints on the Andean uplift from u–pb and hf isotopic data of detrital zircons. *Tectonophysics* **489**(1–4), 258 – 273. URL http://www.sciencedirect.com/science/article/pii/S0040195110001642.

Wiens, D. A. & Stein, S. (1985). Implications of oceanic intraplate seismicity for plate stresses, driving forces and rheology. *Tectonophysics* **116**(1-2), 143 – 162. URL http://www.sciencedirect.com/science/article/pii/0040195185902276.

Zhong, S. & Leng, W. (2006). Dynamics of mantle plumes and their implications for the heat budget and composition of the mantle. *Geochimica et cosmochimica acta* **70**(18, S), A749.

Appendix A

Geologic time scale

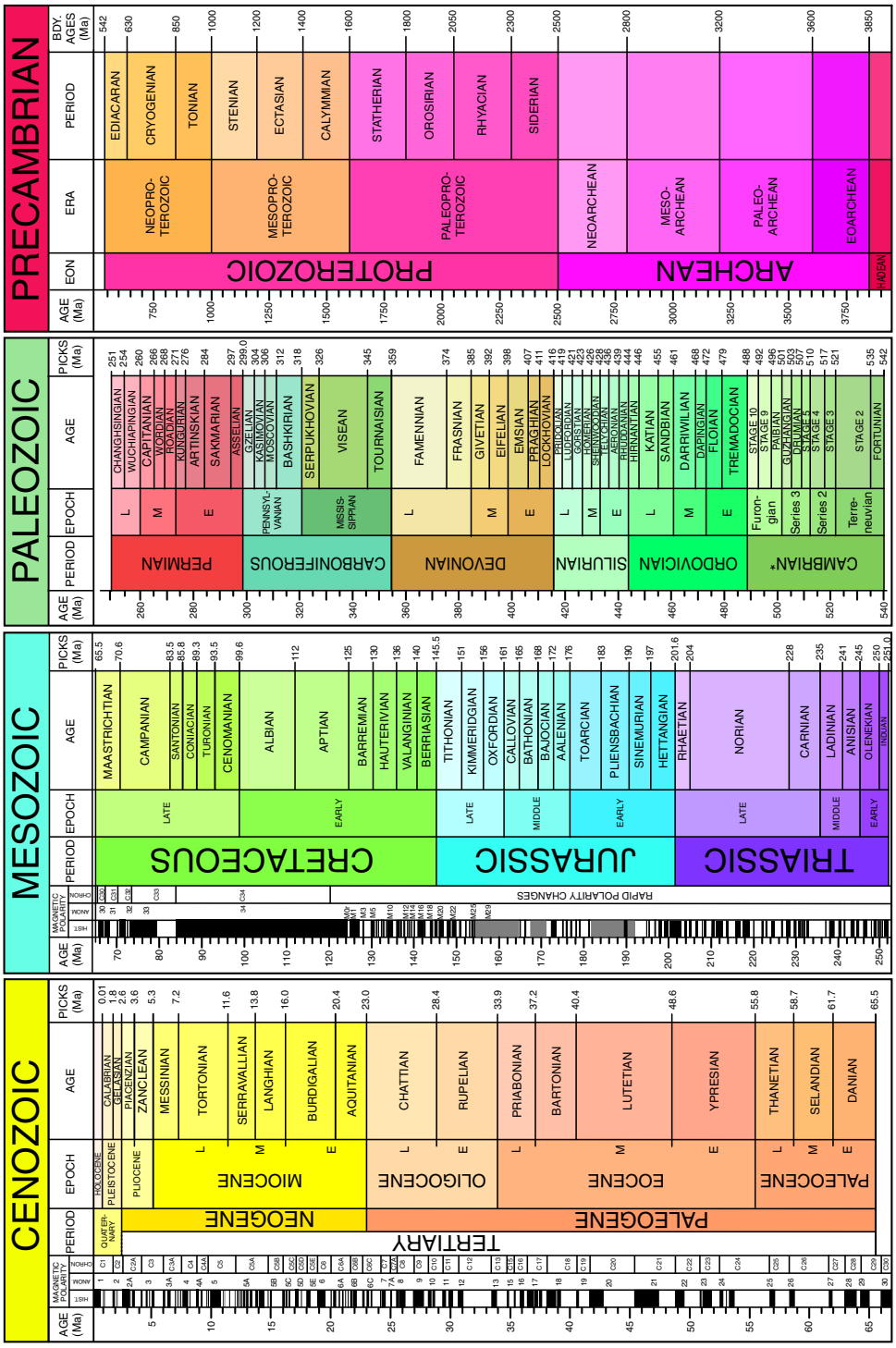

*International ages have not been fully established. These are current names as reported by the International Commission on Stratigraphy.

Walker, J.D., and Geissman, J.W., compilers, 2009, Geologic Time Scale: Geological Society of America, doi: 10.1130/2009.CTS004R2C. ©2009 The Geological Society of America.
Sources for nomenclature and ages are primarily from Gradstein, F., Ogg, J., Smith, A., et al., 2004, A Geologic Time Scale 2004: Cambridge University Press, 589 p. Modifications to the Triassic after: Furin, S., Preto, N., Rigo, M., Roghi, G., Gianolla, P., Crowley, J.L., and Bowring, S.A., 2006, High-precision U-Pb zircon age from the Triassic of Italy: Implications for the Triassic time scale and the Carnian origin of calcareous nannoplankton and dinosaurs: Geology, v. 34, p. 1009–1012, doi: 10.1130/G22967A.1; and Kent, D.V., and Olsen, P.E., 2008, Early Jurassic magnetostratigraphy and paleolatitudes from the Hartford continental rift basin (eastern North America): Testing for polarity bias and abrupt polar wander in association with the central Atlantic magmatic province: Journal of Geophysical Research, v. 113, B06105, doi: 10.1029/2007JB005407.

THE GEOLOGICAL SOCIETY OF AMERICA®

Appendix B

Mantle convection

We will look at the equations that governs mantle convection in order to see the maximum change in the velocity rate that mantle convection can explain. A starting point for describing the physics of a continuum are the conservation equations. For what concerns, the momentum conservation equation. The changes of momentum can be easily deduced by balancing it with the body forces acting in a volume Ω and the surface force acting on its surface Σ, that is, Newton's second law. The total momentum is,

$$\int_\Omega \rho\vec{v}dV$$

and its variations are due to advective transport of momentum across the surface, forces acting on this surface and internal body forces. The momentum conservation of an open, fixed volume, can therefore be expressed in integral form as

$$\int_\Omega \frac{\partial(\rho\vec{v})}{\partial t}dV = -\int_\Sigma \rho\vec{v}(\vec{v}\cdot d\vec{S}) + \int_\Sigma \underline{\sigma}\cdot d\vec{S} + \int_\Omega \vec{F}dV \tag{B.1}$$

The tensor $\vec{\sigma}$ corresponds to the total stresses applied on the surface Σ. Our convention is that σ_{ij} is the i component of the force per unit area across a plane normal to the j-direction. The term $\vec{F}$ represents the sum of all body forces, and in particular the gravitational forces ρg.

Using the divergence theorem for the first term on the right-hand side, $\rho\vec{v}(\vec{v}\cdot d\vec{S})$ can also be written $\rho(\vec{v}\otimes d\vec{S})$ and knowing the mass conservation equations for any vector field $\vec{A}$,

$$\frac{\partial\vec{A}}{\partial t} + \nabla\cdot(\rho\vec{A}\otimes\vec{v}) = \rho\frac{D\vec{A}}{Dt}$$

The differential form the momentum conservations equation becomes,

$$\rho\frac{D\vec{v}}{Dt} = \nabla\cdot\underline{\sigma} + \vec{F}$$

It is common to divide the total stress tensor into a thermodynamic pressure $-P\underline{I}$ where $\underline{I}$ is the identity stress tensor, and a velocity-dependent stress tensor $\underline{\tau}$. Without motion, the total stress tensor is thus isotropic and equal to the usual pressure.

In most geophysical literature, it has been assumed that the velocity-dependent tensor has no isotropic component, which means it is traceless. In this case the thermodynamic pressure P is the average isotropic stress, $tr(\underline{\sigma}) = -3P$, which is not the hydrostatic pressure. The velocity-dependent stress tensor $\underline{\tau}$ is thus also the deviatoric stress tensor. As $\nabla\cdot(PI) = \nabla P$, momentum conservation B.1 , in terms of pressure and deviatoric stresses, is

$$\rho\frac{D\vec{v}}{Dt} = -\nabla P + \nabla\cdot\underline{\tau} + \vec{F}$$

This equation is called Navier-Stokes equation with velocity-dependent stress tensor $\underline{\tau}$

$$\underline{\tau} = \underline{\sigma} - \frac{1}{3}Tr(\underline{\sigma})$$

Where,

$$\underline{\sigma} = -P\underline{I} + 2\eta\underline{\dot{\epsilon}}$$

with the assumption of incompressibility and null bulk viscosity.

When the equations governing the dynamics of the problem at hand are known, a method of dimensional analysis becomes available: nondimensionalisazion. It is usually the best choice as the relevant physical parameters appear explicitly in the equations.

We can nondimensionalize the Navier-Stokes equation multiplying by $\frac{U}{2L}$ each member of the equation. In this way we arrived to explicit the Reynolds number Re that is at the denominator of the viscous forces term in the next equation.

$$\rho\frac{D\vec{v'}}{Dt} = -\nabla P' + \nabla^2\frac{\vec{v'}}{Re} + \vec{F'} \tag{B.2}$$

The Reynolds number gives a measure of the ratio of inertial forces to viscous forces and consequently quantifies the relative importance of these two types of forces for the mantle, it is

$$Re = \frac{\rho U L}{\mu}$$

where taking some characteristic numbers for these parameters we have $\rho = 4000\ kg/m^3$, $U = 1\ cm/yr$, $L = 6000000\ m$ and $\mu = 10^{21}$ P as, the Reynolds number for the Earth results very small, thus the term of the inertia forces in equation B.2 ($\frac{D\vec{v'}}{Dt}$) is negligible and we arrive to the Stokes equation for a laminar flow.

$$0 = -\nabla P' + \nabla^2\frac{\vec{v'}}{Re} + \vec{F'}$$

If we solve for $\vec{v}$ we see that the solution for this equation is a stationary one. It is stationary because the parameters are not time-dependent.

We speculated to solve the Stokes equation for the motion of a spherical anomaly of temperature in an uniform, infinite and homogeneous space. The fluid sphere has radius a and viscosity η_1 in an unbounded fluid with viscosity $\eta_0 = \frac{\eta_1}{\gamma}$ (where γ is the ratio of the viscosity of the sphere to that of the surrounding fluid) and velocity $U\vec{e}_z$ far from the sphere. The drag on the sphere is

$$\vec{F} = 4\pi\alpha\eta_0 U \frac{1+3\gamma/2}{1+\gamma}\vec{e}_z$$

If the densities of the two fluids differ such that $\rho_1 = \rho_0 + \Delta\rho$, the steady velocity of the sphere $\vec{V}$ as it moves freely under gravity is obtained by equating $\vec{F}$ to the Archimedean buoyancy force,

$$\vec{V} = \frac{a^2\vec{g}\Delta\rho}{3\eta_0}\frac{1+\gamma}{1+3\gamma/2} \tag{B.3}$$

The speed of an effectively inviscid sphere ($\gamma = 0$) is only 50 percent greater than that of a rigid sphere ($\gamma \to \infty$).

Equation B.3 has been widely used to estimate the ascent speed of plume heads in the mantle. Considering $a = 500000$ m that is a typical dimension of a mass anomaly, a density variation around 1 since we consider $\alpha = 10^{-5}\ 1/K$ and $\nabla T = 10^2\ K$ in $\rho = \rho_0(1 + \alpha\nabla T)$, and a viscosity $\mu = 10^{21}$ P as. As a result we obtain a velocity of 1 cm/yr, this means that material in the mantle is flowing at around 1 order of magnitude lower than observed plate motions.

So far we considered the paramaters in the equations as constant parameters and so the velocity we found is a stationary solution. But we know that the temperature gradient causes a density variation and so the gravitational forcing is time-dependent.

Thus, to have an estimate of the rate with which the speeds in the mantle change, we must not look only at the Stokes equation, but we must look at Stokes equation coupled with the Energy equation that rules the evolution of the temperature anomalies. We want to investigate on what time-scale, from an Eulerian point of view, the temperature anomalies change sensibly. For what concerns the energy conservation, the total energy per unit mass of a fluid is the sum of its internal energy U and its kinetic energy. In the fixed volume Ω, the total energy is thus

$$\int \rho\left(U + \frac{\vec{v}^2}{2}\right) dV$$

A change of the energy content can be caused by: advection of energy across the boundary σ by macroscopic flow, transfer of energy through the same surface without mass transport, by say diffusion or conduction, work of body forces, work of surface forces and volumetrically distributed radioactive heat production. Using the divergence theorem, the balance of energy can therefore be written as

$$\frac{\partial}{\partial t}\left(\rho\left(U+\frac{v^2}{2}\right)\right)=-\nabla\cdot\left(\rho\left(u+\frac{v^2}{2}\right)\vec{v}+\vec{q}+P\vec{v}-\underline{\tau}\cdot\vec{v}\right)+\vec{F}\cdot\vec{v}+\rho H$$

where $\vec{q}$ is the diffusive flux, H the rate of energy production per unit mass, and where the stresses are divided into thermodynamic pressure and velocity dependent stresses. This expression can be developed and simplified by using the equation of mass conservation for any scalar vector and momentum conservation equation, the concept of lagrangian derivative, in this way we reach the form

$$\rho\frac{DU}{Dt}=\nabla\cdot\vec{q}-P\nabla\cdot\vec{v}+\underline{\tau}\colon\nabla v+\rho H$$

The viscous dissipation term $\underline{\tau}\colon\nabla v$ is the contraction of two tensors $\vec{\tau}\,\Delta V$ and V (of components $\frac{\partial v_i}{\partial x_j}$). Its expression is $\Sigma_{ij}\tau_{ij}\partial v_i/\partial x_j$. Through some thermodynamic considerations, we arrive to the relation

$$\frac{DU}{Dt}=C_p\frac{DT}{Dt}-\frac{\alpha T}{\rho}\frac{DP}{Dt}-\frac{\nabla\cdot\vec{v}}{\rho}$$

Where C_p is the specific heat capacity and measures the capacity of the material to hold heat at constant pressure. We can employ this thermodynamic relation, in our conservation equations for fluid mechanics, to express the conservation of energy in terms of temperature variations.

$$\rho C_p\frac{DT}{Dt}=-\nabla\cdot\vec{q}+\alpha T\frac{DP}{Dt}+\vec{\tau}\colon\nabla v+\rho H$$

We observe that the Lagrangian variation of temperature in time is due to four elements: the four elements in the right side of the equation. They are respectively heat conduction, adiabatic transformation, viscous friction and radioactive heat generation. If we explicit the Eulerian and Lagrangian derivative

$$\frac{D}{Dt}=\frac{\partial}{\partial t}+(\vec{v}\cdot\nabla)$$

We find another term that is the advective term $(\vec{v}\cdot\nabla)T$

$$\rho C_p\frac{DT}{Dt}=\rho C_p\left(\frac{\partial T}{\partial t}+(\vec{v}\cdot\nabla)T\right)$$

so,

$$\rho C_p\left(\frac{\partial T}{\partial t}+(\vec{v}\cdot\nabla)T\right)=-\nabla\cdot\vec{q}+\alpha T\frac{DP}{Dt}+\vec{\tau}\colon\nabla v+\rho H \tag{B.4}$$

If we estimate the order of magnitude of all the terms in the equation B.4 we see that the most impactive term is the advective one. In the heat conduction term $\vec{q}$ is $k\nabla T$ and knowing that we have a change in temperature of 3000 K in 3000 km (from the CMB to the upper mantle) we see that this term is of the order of 10^{-15}, in the adiabatic transformation term we take the temperature around 2000 K and we know that in average in 100 Ma we have a 40 GPa of change in pressure if we consider 1000 km, this term is of the order of magnitude of 10^{-8}. The viscous friction term is of the order of magnitude of 10^{-11} since $\vec{\tau}=\mu\nabla v$ and we see that $\nabla v\approx 10^5$. The radioactive heat generation term is of the order of magnitude of 10^{-10} since the rate of energy production per unit mass is 10^{-13} and $\rho\approx 4000kg/m^3$. The

advective one is of the order of magnitude of 10^{-4}, since $v \approx 10^{-10} m/s$ and the temperature variation was already discussed. The variation in time of gravitational forcing is principally due to advection of the very gravity from convection, only secondly it is due to its creation/dissipation through heat conduction or radioactive heating.

The advective term is given by the scalar multiplication between velocity and temperature gradient. Since diffusion and heat generation are secondary phenomena, the temperature gradient remains basically unchanged in intensity, it is simply shifted from one side to the other in the mantle by the macroscopic shift of material. Now, if we want to understand which change in velocity mantle convection can explain, we must find how fast this temperature gradient is brought up. Since a typical mass anomaly in the mantle is around $500km$ wide and it moves 1 cm/yr, as calculated previously, it would be needed a time of 100 Ma to have $\Delta v = 1$ cm/yr.

Appendix C

Andean geology table

Table C.1: Table containing the geological information

Article	Data type	Place	Time	Description
Aragon *et al.* (2011)	-	Southern Andes, Patagonia	Late Cret. to Danian	Development of the Proto-Andean range.
			M. Eocene to M. Oligocene	Delopment ed the Northern Patagonian High Plateau.
			L. Oligocene to E. Miocene	Proto-Andean underwent major erosion.
Arriagada *et al.* (2008)	Shortening	Bolivian Orocline s	Eocene-Oligecene	Formed as a consequence of differential horizontal shortening.
Barnes *et al.* (2006)	AFT, ZFT and (U–Th)/He	E. Cordillera s	40 - 25 Ma	Accelerated erosion.
			since 15 Ma	Distributed erosion across the entire thrust belt.
Charrier *et al.* (2007)	Stratigraphic data	Arc domain between Antofagasta and Illapel	Early to Late Cretaceous	Extensional regimen.
			Late Cret. Early Paleocene	K-T tectonic event.
			During Paleocene	Extension resumed, but with less intensity.
Cobbold & Rossello (2003)	AFT and Volcanism	Southern Andes, Neuquen basin	Aptian to present	Folding and Thrusting scrrelates to Peruvian Incaic and Quechua phases.
Ege *et al.* (2007)	AFT and ZFT	Central Orocline	33- 27 Ma	Plateau exhumation.
Farías *et al.* (2008)	AFT, see fig. 10 and 2 from the article	Central Andes, 33 to 35 S,	8.5 - 4 Ma	The principal and Eastern Coastal Cordillera were uplifted.
			4 to present	The coastal cordillera and the offshore zone were uplifted.
Garzione *et al.* (2006)	Oxygen isotope Paleogeography	Central Andes, Altiplano	10 - 7 Ma	Uplifted 2.5 to 3.5 km.

Continued on next page

Table C.1 – continued from previous page

Article	Data type	Place	Time	Description
Gillis *et al.* (2006)	ZFT	Central Andes, Altiplano	45 - 40 Ma to 26 Ma	Rapid cooling.
			since 11 Ma	Rapid cooling.
Gregory-Wodzicki (2000)	Deformation, Marine and Coastal facies, Volcanic history, Clima history and Erosion history	W. Cordillera	25 - 18 Ma	Half of its actual elevation.
		Altiplano	$\sim$ 20 Ma	30% of its actual elevation.
			$\sim$ 10 Ma	50% of its actual elevation.
		E. Cordillera	$\sim$ 14 Ma	30% of its actual elevation.
			$\sim$ 10 Ma	50% of its actual elevation.
		Columbian Andes	14 - 5 Ma	40% of its actual elevation.
			5 - 2 Ma	its elevation increased rapidly.
Hartley (2003)	Sedimentological data	Central Andes	15 - 4 Ma	Semiarid to arid.
			4 - 3 Ma	Super arid.
			3 - 0 Ma	Hiper aridity.
Hoorn *et al.* (2010)	AFT	Peruvian Andes	65 - 33 Ma	Mountail hills ($\sim$ 1000 to 2000 m).
			33 - 23 Ma	Mountail hills ($\sim$ 1000 to 2000 m) + Alpine ($<$ 3000 m).
			23 - 10 Ma	Mountail hills ($\sim$ 1000 to 2000 m) + Alpine ($<$ 3000 m) + Marine intrusion.
			10 - 7 Ma	Mostly Alpine ($<$ 3000 m)
			7 - 2 Ma	Alpine ($<$ 3000 m)
Horton (2005)	sediment accumulation, and provenance	Central Andes, 17 -21 S, Eastern Cordillera	25-21 Ma	Inter-montane basin fill starts in latest Oligocene - early Miocene, being deposited in angular unconformity.
Jaillard (1994)	Sedimentary data	Northern Peru	$\sim$ 89-88 Ma (Peruvian Phase 1)	beginning of coastal uplift and inversion of subsidence.

Continued on next page

Table C.1 – continued from previous page

Article	Data type	Place	Time	Description
			∼ 87- 86 Ma (Peruvian Phase 2)	Incipient thrusting and tectonic activity are related to a NE-SW compressional strain.
			∼ 76-73 Ma (Peruvian Phase 3)	Uplift and erosion of the Coastal Cordillera and subsidence of the coastal Area.
Jaillard & Soler (1996)	Sedimentary data	Northern Peru	Late Campanian	Major contractional phase.
		See fig 1 in the article.	Late Eocene (∼ 35 Ma)	folding and reverse faulting in the former Western Trough, formed a fold and thrust belt.
McQuarrie *et al.* (2008)	apatite and zircon fission track cooling ages	Central Andes 15 - 17 S	40 - 25 Ma	Fast exhumation rate in the Eastern Cordillera.
			15(8) - 0 Ma	Rapid exhumation in the entire fold-thrust belt.
			25 - 15(8) Ma	pause or a dramatic deceleration in the rate of deformation and propagation of the fold-thrust belt.
Mpodozis *et al.* (2005)	-	Atacama basin	Late Cretaceous	Uplift in the Cordillera de Domeyko, reflected in the sedimentation in the Salar de Atacama.
		Pedernales basin		Uplift and unroofing of the Cordillera de Domeyko, due to high sedimentation rates.
Picard *et al.* (2008)	Biotaxa (wild potato and tomato)	Southern Peru	23 - 19 Ma	where above 2-2.5 km high.
		Central Peru	16 - 13 Ma	Uplifted above 2-2.5 km
		Northern Peru	since 6 Ma	Uplifted above 2 km
Sempere *et al.* (1990)	-	Bolivia Orocline	late Oligocene	Mayor tectonic crisis.
Sempere *et al.* (1994)	-	32^{o}S - 37^{o}S	27 Ma	Initiation of a major deformation in the Volcanic and Principal Cordillera.
			20 Ma	Volcanic information suggest a quiescent state.

Continued on next page

Table C.1 – continued from previous page

Article	Data type	Place	Time	Description
			since 10 Ma	2 km of uplift in the Aconcagua region.
Sempere *et al.* (1997)	stratigraphy, magnetostratigraphy, Ar/Ar dating, and paleontology	Bolivia and northwest Argentina	∼89 Ma	tectonic event marked a turning point in Andean evolution.
			∼59.5 – 58.2 Ma	Tectonic event marks the initiation of continental foreland sedimentation in Andean Bolivia.
Thomson (2002)	Fission track thermochronology	Patagonian Andes 42-46 S	16 - 10 Ma	Initiation of denudation.
			7 - 2 Ma	Fast denudation.
Tunik *et al.* (2010)	Fission track and U-Pb detrical zircons	Neuquen Basin	98 - 88 Ma	Began Andean Uplift.

Appendix D

Force balance results

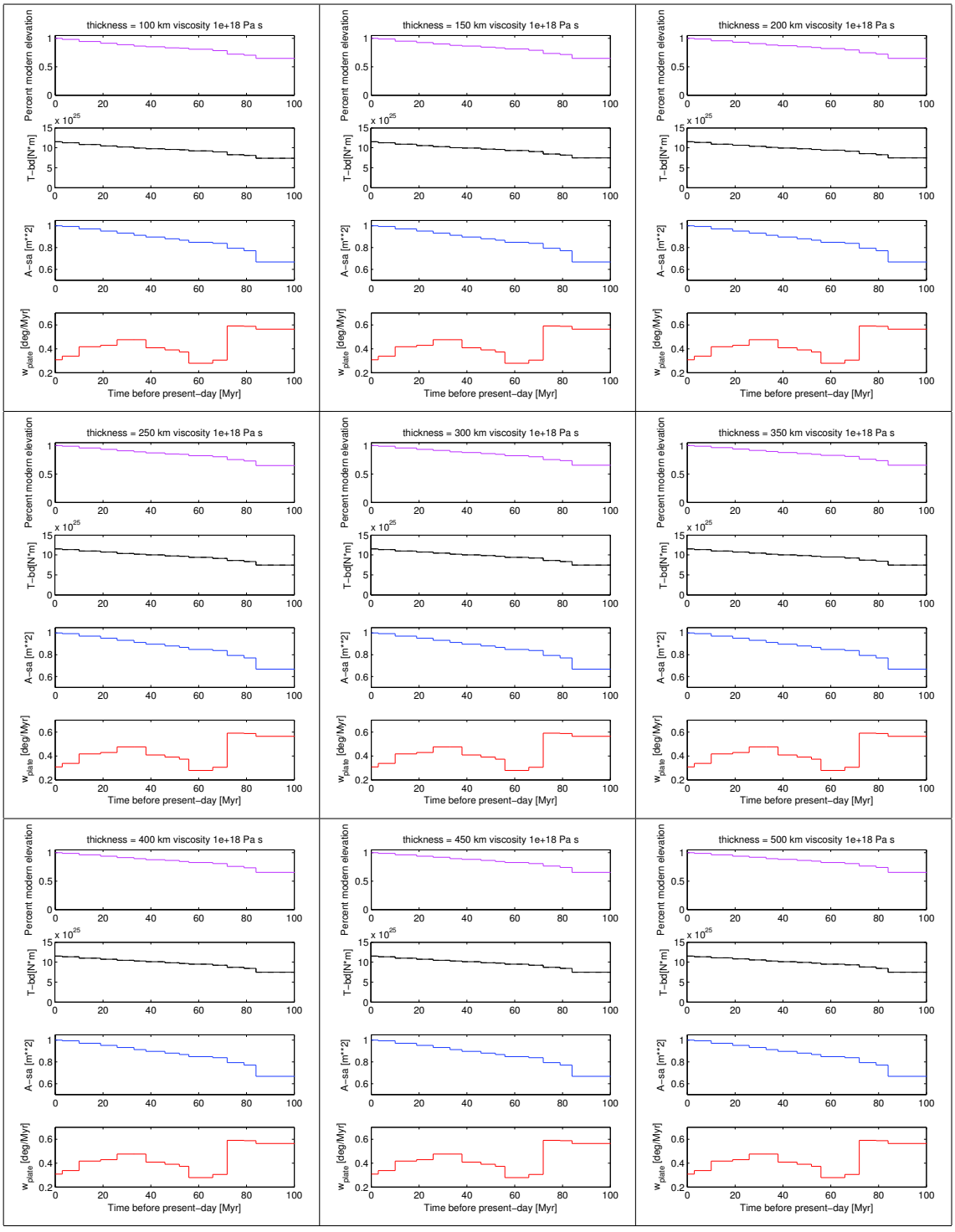

Figure D.1: *Evolution of the South American plate since 100 Ma. All 9 figures show a viscosity of* 1×10^{18} *Pa s and all the combinations of channel thickness (see table 4.1). In each Figure from top to bottom: Average elevation of the Andean Margin with respect to present day, basal shear tractions exerted by the asthenosphere, size of the South American plate and South American plate velocity.*

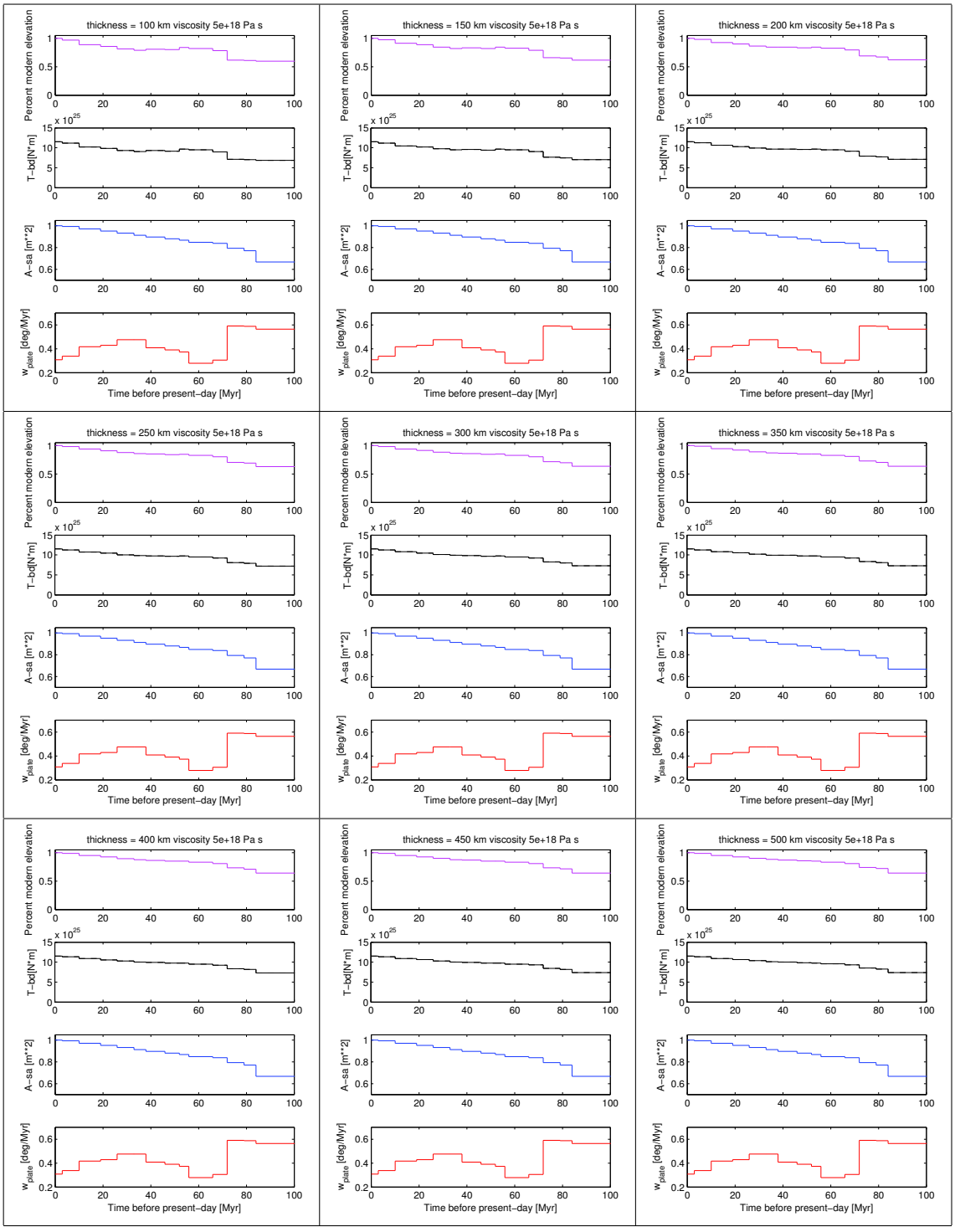

Figure D.2: *Evolution of the South American plate since 100 Ma. All 9 figures show a viscosity of* 5×10^{18} *Pa s and all the combinations of channel thickness (see table 4.1). In each Figure from top to bottom: Average elevation of the Andean Margin with respect to present day, basal shear tractions exerted by the asthenosphere, size of the South American plate and South American plate velocity.*

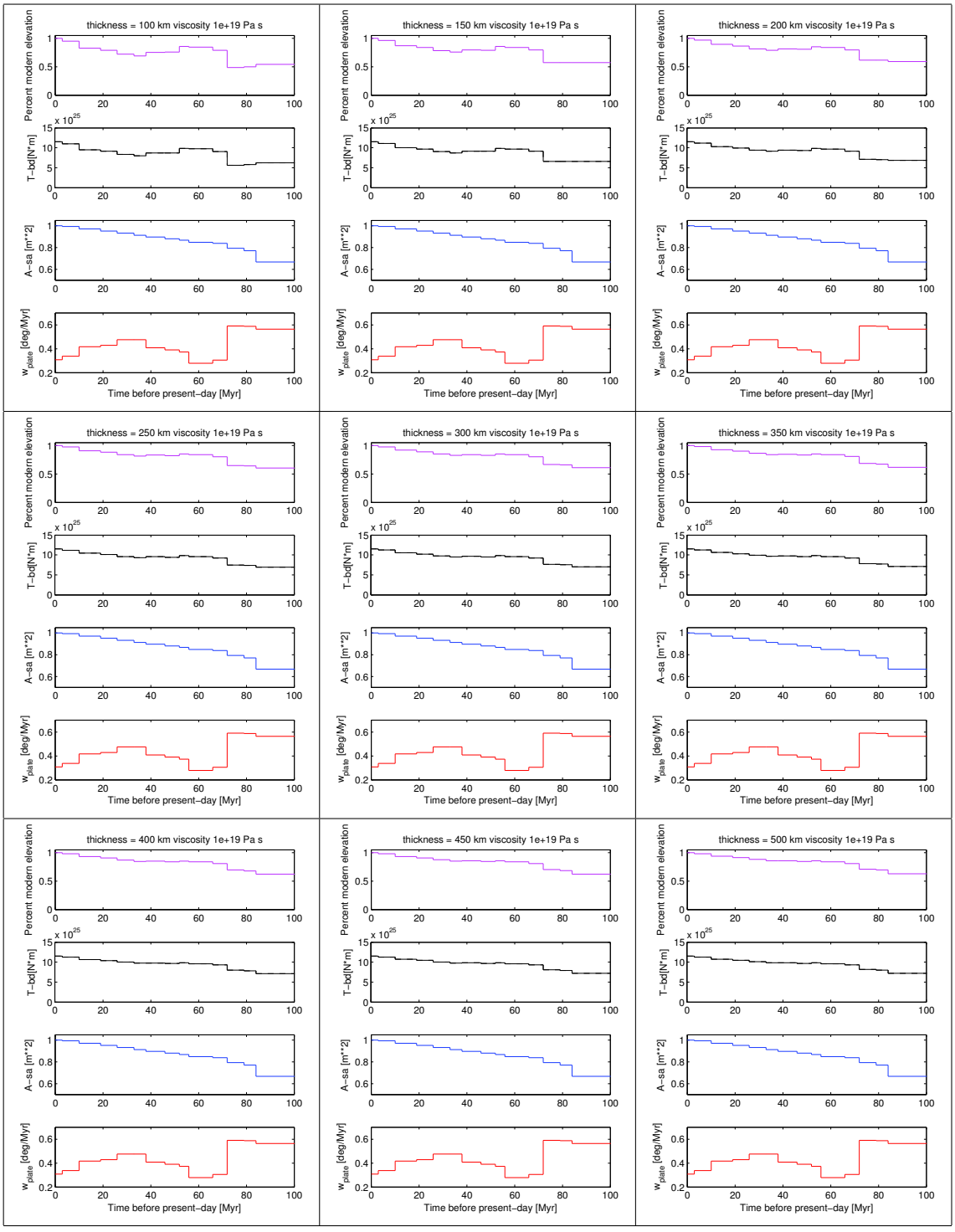

Figure D.3: *Evolution of the South American plate since 100 Ma. All 9 figures show a viscosity of* 1×10^{19} *Pa s and all the combinations of channel thickness (see table 4.1). In each Figure from top to bottom: Average elevation of the Andean Margin with respect to present day, basal shear tractions exerted by the asthenosphere, size of the South American plate and South American plate velocity.*

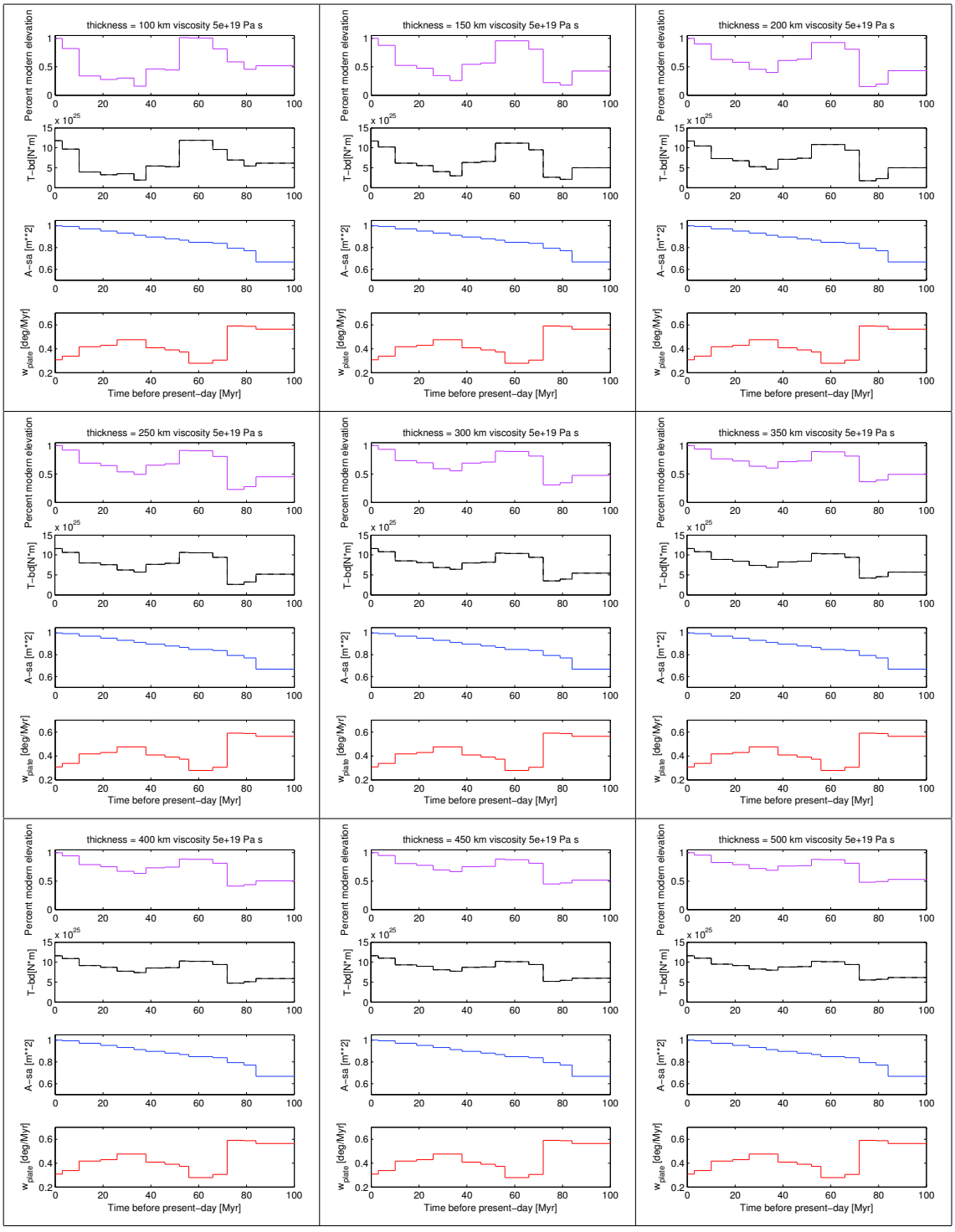

Figure D.4: *Evolution of the South American plate since 100 Ma. All 9 figures show a viscosity of* 5×10^{19} *Pa s and all the combinations of channel thickness (see table 4.1). In each Figure from top to bottom: Average elevation of the Andean Margin with respect to present day, basal drag shear tractions by the asthenosphere, size of the South American plate and South American plate velocity.*

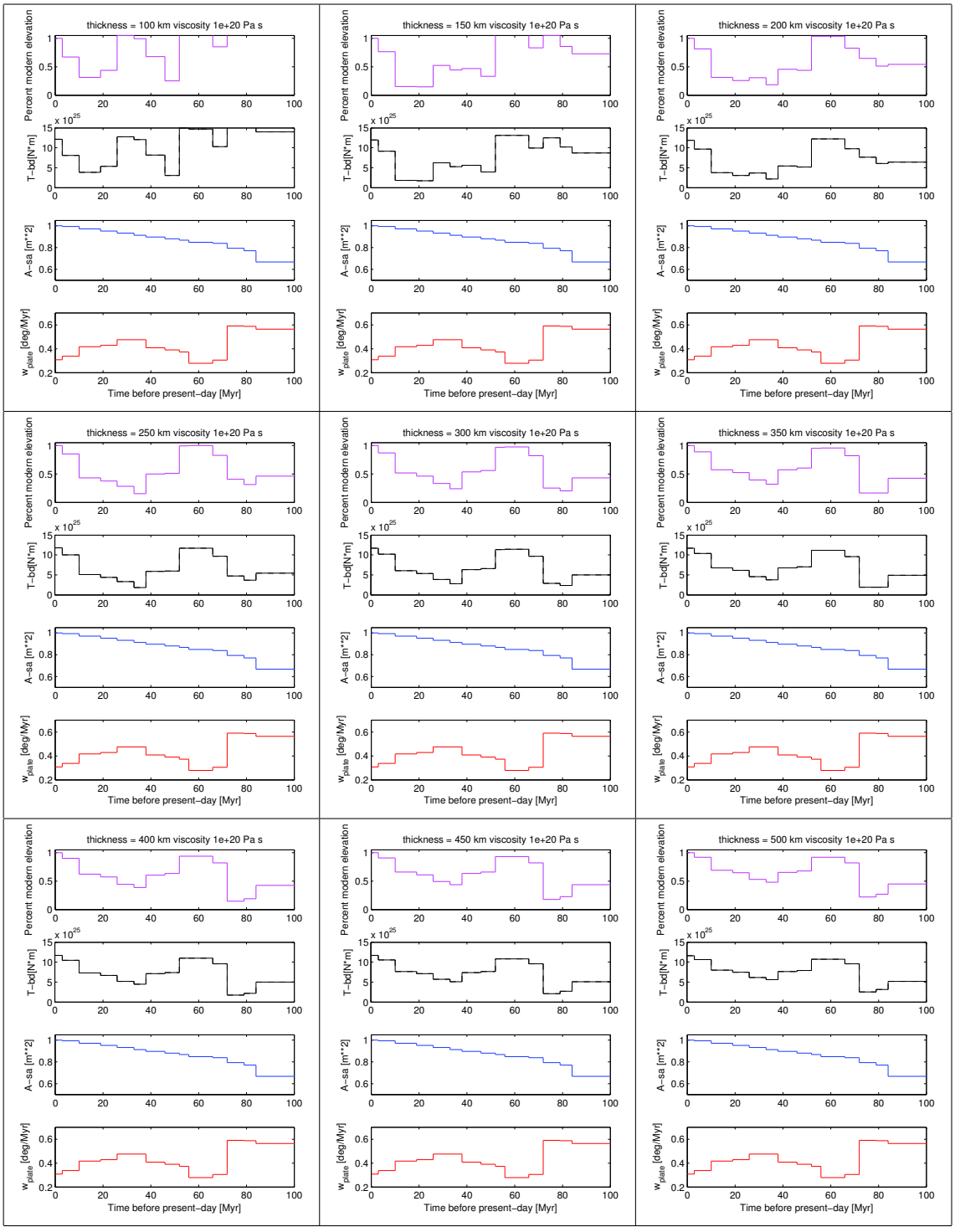

Figure D.5: *Evolution of the South American plate since 100 Ma. All 9 figures show a viscosity of* 1×10^{20} *Pa s and all the combinations of channel thickness (see table 4.1). In each Figure from top to bottom: Average elevation of the Andean Margin with respect to present day, basal shear tractions exerted by the asthenosphere, size of the South American plate and South American plate velocity.*